Robust Control of Large Scale Power Systems

Final Project Report

Power Systems Engineering Research Center

A National Science Foundation
Industry/University Cooperative Research Center
since 1996

Power Systems Engineering Research Center

Robust Control of Large Scale Power Systems

Final Report

Vijay Vittal, Project Leader
Iowa State University

Project Team

Mustafa Khammash, Chuanjiang Zhu, Wenzheng Qiu
Iowa State University

Peter Young, Rod Holland
Colorado State University

Christopher DeMarco
University of Wisconsin-Madison

PSERC Publication 02-43

November 2002

Information about this Project

For information about this project contact:

Vijay Vittal
Harpole Professor
Iowa State University
Department of Electrical and Computer Engineering
1126 Coover Hall
Ames, IA 50011
Phone: 515-294-8963
Fax: 515-294-4263
Email: vvittal@iastate.edu

Power Systems Engineering Research Center

This is a project report from the Power Systems Engineering Research Center (PSERC). PSERC is a multi-university Center conducting research on challenges facing a restructuring electric power industry and educating the next generation of power engineers. More information about PSERC can be found at the Center's website: http://www.pserc.wisc.edu.

For additional information, contact:

Power Systems Engineering Research Center
Cornell University
428 Phillips Hall
Ithaca, New York 14853
Phone: 607-255-5601
Fax: 607-255-8871

Notice Concerning Copyright Material

Acknowledgements

The work described in this report was sponsored by the Power Systems Engineering Research Center (PSERC). We express our appreciation for the support provided by PSERC's industrial members and by the National Science Foundation under grant NSF EEC-9908690 received under the Industry/University Cooperative Research Center program.

Our thanks are also given to Hydro-Quebec and MidAmerican Energy for its support of this project. Thanks are also given to the following individuals who contributed to this project as our industry advisors:

Miodrag Djukanovic	MidAmerican Energy Co.	Industry advisor
Innocent Kamwa	Institut de recherche d'Hydro-Quebec (IREQ)	Industry advisor

Executive Summary

This research is concerned with the problem of power system control under uncertainty. Power systems must typically perform over a wide range of operating conditions. For instance, the load demands at a certain bus can vary gradually, or even sharply, every hour throughout a day; disturbances of differing extents of severity could happen during the normal operation; and the topology of the system could change over time. The existence of uncertainties requires good robustness of the control systems. A control system is robust if it is insensitive to differences between the actual system and the model of the system that was used to design the controller. These differences are referred to as model/plant mismatch or simply as model uncertainty. As for power systems, the control system will have to regulate the system under diverse operating conditions; it must have the ability to tolerate model uncertainties, suppress potential instability, and damp the system oscillations that might threaten system stability when the system is operating under stressed conditions.

One of the major tasks in the design of control systems in a power system is to evaluate the stability robustness. Conventional controllers are designed to make the system stable under a specific operating condition. Time domain simulations are then used to evaluate the controller at specific points in a range of operating conditions. The simulation obviously cannot cover the whole operating range; thus, the resulting evaluation procedure cannot guarantee robustness of the controller over the whole range.

Modern robust control theories have been developed significantly in the past years. The key idea in a robust control paradigm is to check whether the design specifications are satisfied even for the "worst-case" uncertainty. Many efforts have been taken to investigate the application of robust control techniques to power systems. Among them, H_∞ optimization techniques have many applications in power systems. But the additive and/or multiplicative uncertainty representation not only overbounds the parametric uncertainty but also has the restriction to treat situations where a nominal stable system becomes unstable after being perturbed. Moreover, a very important procedure in the H_∞ design is to choose weighting functions. This is by no means easy and requires practice. In addition, the order of the resulting H_∞ controller is as high as that of the plant.

Structured Singular Value (or μ) based tools have been proven to be promising. They were introduced to take advantage of the fact that in many problems uncertainty can be represented in a structured form, e.g., a block-diagonal form. Algorithms were developed to compute upper and lower bounds for μ, and the computed bounds were usually tight enough for practical applications. This has lead to a significant reduction in conservatism over methods that simply lump all uncertainty into a single, norm-bounded block. The μ approach, however, involves complex computation. It encounters difficulty in application to large-scale systems due to the heavy computational burden. It has been shown that the mixed μ problem is NP hard, which means that no algorithm can evaluate μ in polynomial time. This property of the problem suggests that instead of trying to evaluate the exact μ, a more practical approach would be to evaluate good bounds. In fact, even the calculation of bounds takes considerable time. Thus, it is desirable to propose feasible algorithms to perform the bounds calculation. The research

conducted in this project extends existing methods to more practical algorithms for achieving the μ bounds to deal with the robustness analysis problem in power systems.

A major portion of the computational burden in evaluating the bounds on μ arises from having to conduct a gridded sweep over the frequency range of interest. Treating the frequency as an uncertainty and reformulating the problem with an augmented uncertainty block overcomes this drawback. We refer to this formulation as the skewed-μ approach. We have formulated the problem of designing controllers for power systems as a skewed-μ problem. Using the skewed-μ approach we have developed an efficient branch and bound to determine the supremum of μ. This is a key step in the analysis. This scheme is very effective and significantly reduces the computational burden. The formulation developed has worked efficiently in the test systems considered. It significantly reduced the computation time in evaluating the peak value of μ. As a result, the robustness analysis was performed efficiently.

Two other important bound determination techniques are also developed based on the skewed-μ formulation. These include efficient evaluation of the skewed-μ lower and upper bounds. The analytical basis for the computation of the bounds has also been developed. In addition, efficient algorithms are developed to evaluate the skewed-μ lower and upper bounds. These algorithms have been implemented using the Matlab μ-tool box. These algorithms are then tested on realistic power systems. The results obtained demonstrate that the analytical basis for the development of the skewed-μ bounds is sound. The algorithms developed to determine the skewed-μ bounds utilize associated algorithms like the Matlab LMI tool box that are not as efficient for large power systems. Specific algorithms to perform these special purpose algorithms for large power systems need to be developed. This is a topic for future research.

With the focus on control design techniques that are computationally efficient and the need to effectively design controls with the desired robustness and performance capabilities, we examined other possible design techniques. A newly developed technique called H_∞ loop-shaping was identified and carefully studied. The technique is first formulated for the power system problem and then applied to design controls for a wide range of operating conditions. The designed controls are then tested using nonlinear simulations.

In this project we specifically applied the technique to design power system stabilizers (PSS) for multi-machine systems. The problem of designing the PSS was first formulated. Uncertainties arising from changing operating conditions were characterized. The PSS design at each machine was then cast as a sequential control design problem as follows:

> A particular location is first chosen to design the PSS. The different modal frequencies are examined and loop shaping is done around desired frequencies to obtain the desired gain. H_∞ design is then done taking into account the uncertainties. The resulting controller is typically of higher order. Appropriate model reduction techniques are used to obtain controllers that can be practically implemented. The designed controller is then folded into the system and the PSS at the next location is designed.

This procedure has significant advantages since the design of new controllers is done taking into account the controllers that were designed in the previous steps. As a result, we can account for

the interaction between controllers. The results of the testing again demonstrate the efficacy of the method and the simplicity in applying it to large power systems.

The techniques developed in this project are tested on two standard test systems. These include a 4-Generator test system specifically designed to test the efficacy of the controller in damping inter-area oscillations and a 50-Generator IEEE test system that exhibits complex dynamic behavior. The designed controllers are tested over a wide range of operating conditions and their performance is verified using nonlinear time domain simulations.

The design of the power system stabilizer using the proposed approach has been tested on a realistic power system model. The approach developed is fairly general and, without loss of generality, can be applied to the design of a wide range of controllers including excitation control, governor control, and controllers for FACTS elements. Among these, the controllers for FACTS elements have tremendous application potential. These controllers could include HVDC controls and controllers for static var systems. Accounting for uncertainty and change in network conditions will greatly benefit the design of controllers for FACTS elements since these elements are strategically located in the network and have the capability to make significant changes in network power flow. This is in contrast with conventional controllers that are generally designed to control synchronous machine variables. In addition FACTS controllers installed in the network are likely to see a greater variation in operating conditions due to the changes in interface flows and increased transactions. In such situations, the proposed design procedure that accounts for the uncertainty can effectively provide a design that satisfies both robust stability and performance requirements. This will significantly enhance the utility of FACTS devices that, in addition to their primary control function, can also provide significant improvement in system dynamic performance.

Supplementary controllers associated with FACTS elements could be effectively designed to damp large inter-area oscillations and allow higher transaction levels to take place. One approach to achieve this goal is to use a supplementary damping controller in association with a static var compensator (SVC). Using the robust control approaches presented in this report, a supplementary controller can be designed to take into consideration a wide range of operating conditions and damp out inter-area oscillations in addition to performing the primary function of voltage control. In doing the design, the robust design procedure can be effectively used to select the supplementary controller signals and also to select the ideal location for the SVC. The algorithms developed in this project for large systems can be effectively utilized to perform the design on realistic systems. The procedure will also account for all the existing controls in the system and take into consideration the interaction between the different types of controls.

The techniques developed in this project can also be applied to the design of unified power flow controllers (UPFCs). This topic is of great interest to several utility companies. The ability to design under uncertain conditions and also apply it to a large scale system is the primary advantage of the developed technique. The project has shown that a systematic design procedure can be established to account for changing operating conditions and also account for interaction between different controls. The ability of the obtained designs to enhance operating limits has also been shown. Hence, the application of the developed procedure to design controls for new devices that are just finding acceptance in the industry will be an excellent proving ground.

Another important follow-up to this project would be to demonstrate the efficacy and advantages of the design tools developed on real specific design examples identified by engineers at PSERC member companies. The investigators would also consider providing a short course on the design techniques and developing hands-on demonstrations to show how the tools developed can be easily used to accomplish design tasks.

Table of Contents

1 An Introduction to Structured Singular Value (SSV)

In this section a brief overview of the structured singular value approach to robust analysis of controls is provided. The advantages of the technique will be highlighted. In addition, the computational burden imposed by the technique on large systems will be discussed and approaches to overcome the computational burden will be presented.

1.1 Uncertainty characterization

Over the years, precise and fixed linear control schemes have been used extensively in many engineering applications. These kinds of designs do not take into account the uncertainties that could be encountered in both the plant and controller models. The uncertainty may have several origins.

1. There are many parameters in the linear model which are only known approximately or are simply in error.
2. The parameters in the linear model may vary due to changes in the operating conditions.
3. Measurement devices cause errors.
4. There are neglected dynamics when simplifying the system model.
5. Uncertainties can be caused by the controller model reduction or by implementation inaccuracies.

The first step of the robust control methodology is to model and bound the above uncertainties in an appropriate way. The next step is to try to design a controller that is insensitive to the difference between the actual system and the model of the system; i.e., a controller that can handle the worst-case perturbations.

In the current literature, modeling of uncertainty is considered from two viewpoints.

- In the frequency domain, the perturbation is considered to be a transfer function, separate from the system model [1]. This kind of uncertainty could be multiplicative or additive. For example, the normalized coprime factor uncertainty in [2] is a kind of additive uncertainty.
- In the state-space representation, the uncertainties in the matrices can be captured.

Those viewpoints are typically used to deal with the parametric uncertainty.

If the uncertainty description represents one or several sources combined together to form a single lumped perturbation of a chosen structure, such uncertainty is called unstructured uncertainty. Parametric uncertainty is usually modeled in a structured way. However, sometimes there can be several levels of structure. For example, when the uncertainties include both parametric uncertainties and unmodeled dynamics, the whole uncertainty block could be a structured one and arranged in a diagonal form while, in particular, each block for the unmodeled dynamics could be a lumped unstructured block. In our research, we focus on the parametric

uncertainties characterized in a structured way, and the uncertainties are captured in a state-space representation context.

In [3], a framework for robust stability assessment of controls in multimachine power systems was used. Starting from the algebraic and differential equations, all the algebraic variables in the component differential equations were eliminated according to the relationship derived from the network algebraic equations. The resulting differential equations were linearized at the nominal operating point to create a simplified linear system. The parametric uncertainties on the elements of the coefficient matrix of the system equations were then characterized by polynomial approximation.

1.2 Computation of the μ bounds

When the uncertainty is characterized in a structured manner, more information about the uncertainty is captured since the unstructured uncertainty is assumed to be bounded but otherwise unknown. In practical problems, it is generally the case that the uncertainty consists of multiple norm-bounded perturbations. Consequently, using only a single norm-bounded perturbation for analysis is rarely adequate.

The structured singular value is defined based on the structured uncertainty representation. It is a function that provides a generalization of the singular value (for a single full complex block) and the spectral radius (for a single repeated complex scalar block). It gives the smallest size of the uncertainty (measured by the maximum singular value of the uncertainty block) which makes the system lose stability. Since it is based on an uncertainty characterization that makes use of much more information than most other robust approaches, it gives much less conservative results.

In practice, the major difficulty in the application of the μ approach lies in the computational burden, especially when the system dimension and the number of uncertain parameters are large. The major issues in computing μ, or its equivalent are the generality of the problem description, the exactness of analysis, and the ease of computation. Many works in the literature deal with the computation of μ bounds. They may be divided into two categories: (1) those methods that emphasize refining the bounds by reducing gaps between the upper and lower bounds as much as possible to achieve high accuracy; and (2) those methods that aim at reducing the computational complexity, which tends to obtain μ quickly at the expense of getting relatively cruder results. To explore the algorithms obtaining μ, we need to make proper trade-offs between accuracy and computation time.

The upper and lower bounds are derived as two optimization problems. The lower bound of μ is derived as a real eigenvalue maximization problem, and an improved power iteration has been developed for the generalized mixed μ case. Although it can be proved that μ is exactly equal to the maximal of this optimization problem, this problem is not convex; in general, only local minima can be achieved instead of global maxima. Thus, usually we can find only the lower bound. The commercial MATLAB Toolbox "μ analysis and synthesis" [4] uses the power algorithm to compute the lower bound. An upper bound was presented by Fan, et. al [5] which involves minimizing the eigenvalues of a Hermitian matrix. We will use these bounds in our calculation.

The general μ analysis procedure is to compute the bounds of $\mu(\omega)$ as a function of frequency ω. In practice, this function is usually computed at each point of a frequency grid. This frequency sweep technique may, however, be unreliable in the case when narrow and high peaks exist on the μ plot, since critical frequencies can be missed.

Doyle in [6] gave a state space test for the fast calculation of μ. This test first performs a bilinear transformation where the frequency variable is treated as another Δ block to give a larger problem that converts the continuous-time μ problem to a discrete time μ problem. Since the bilinear transformation is a one-to-one mapping between the frequency axis and the unit circle, no frequency will be missed. Moreover, this transforms the frequency domain calculation to a single constant μ calculation involving larger M and Δ matrices. This gives a one-shot state-space μ test. But this kind of test does not have the flexibility to evaluate μ over a specified frequency interval and to get the worst-case parameter. It needs a search procedure over a particular variable that is time consuming and usually relies heavily on the tightness of the bounds to give information on the value of the particular variable.

1.3 Definition of μ

Suppose we have a complex matrix $M \in C^{n\times n}$ and three non-negative integers m_r, m_c, and m_C (with $m = m_r + m_c + m_C \le n$), which specify the number of uncertainty blocks of repeated real scalars, repeated complex scalars, and full complex blocks, respectively. Then the block structure $\boldsymbol{K}(m_r, m_c, m_C)$ is an m-tuple of positive integers:

$$\boldsymbol{K} = \left(k_1, \ldots, k_{m_r}, k_{m_{r+1}}, \ldots, k_{m_r+m_c}, k_{m_r+m_c+1}, \ldots, k_m\right) \tag{1.1}$$

This m-tuple specifies the dimensions of the perturbation blocks and determines the set of allowable perturbations:

$$\begin{aligned}\chi_{\boldsymbol{K}} = \{\Delta \mid \Delta = \text{block diag}\left(\delta_1^r I_{k_1}, \ldots, \delta_{m_r}^r I_{k_{m_r}}, \delta_1^c I_{k_{m_r+1}}, \ldots, \delta_{m_c}^c I_{k_{m_r+m_c}}, \Delta_1^c, \ldots, \Delta_{m_C}^c\right): \\ \delta_i^r \in R, \delta_i^c \in R, \Delta_i^c \in C^{k_{m_r+M_C+i}\times k_{m_r+M_C+i}} \ \}\end{aligned} \tag{1.2}$$

This block structure is a general form for any combination of repeated real scalars, repeated complex scalars, and full complex blocks. The purely complex case corresponds to $m_r = 0$, and the purely real case to $m_c = m_C = 0$.

The SSV, $\mu_{\boldsymbol{K}}(M)$ of a matrix $M \in C^{n\times n}$ with respect to a block structure $\boldsymbol{K}\left(m_r + m_c + m_C\right)$, is defined as follows:

$$\mu_{\boldsymbol{K}}(M) = \left[\min_{\Delta \in \boldsymbol{K}} \bar{\sigma}(\Delta) : \det(I - M\Delta) = 0\right]^{-1} \tag{1.3}$$

with $\mu_{\kappa}(M) = 0$ if $\det(I - M\Delta) \neq 0$ for all $\Delta \in \chi_{\kappa}$.

From the definition of μ in (1.3), it is not obvious how the value of μ may be computed. In fact, the exact calculation of μ is generally very difficult [7]. Equation (1.4) provides the lower and upper bounds for μ, however, both bounds are too crude since the gap between them can be arbitrarily large in some cases. In order to reduce the gap, we define the following sets of scaling matrices Q_{κ} and D_{κ}:

$$Q_{\kappa} := \left\{\Delta \in \chi_{\kappa} : \delta_i^r \in [-1,1], \delta_i^{c^*} \delta_i^c = 1, \Delta_i^{C^8} \Delta_i^C = I_{k_{m_r+m_c+i}}\right\} \tag{1.4}$$

$$\begin{aligned} D_{\kappa} := \{&\text{block diag}\left(D_1, \ldots, D_{m_r+m_c}, d_1 I_{k_{m_r+m_c+1}}, \ldots, d_{m_c} I_{k_m}\right): \\ &0 < D_i = D_i^* \in C^{k_i \times k_i}, 0 < d_i \in R\} \end{aligned} \tag{1.5}$$

then the lower bound and upper bound can be refined as

$$\max_{Q \in Q_{\kappa}} \rho_R(QM) \leq \mu_{\kappa}(M) \leq \inf_{D \in D_{\kappa}} \bar{\sigma}\left(DMD^{-1}\right) \tag{1.6}$$

It has been proven in [8] that the first inequality in (1.6) is actually an equality. However, the function $\rho_R(QM)$ is not convex in $Q \in Q_{\kappa}$ and therefore it is not guaranteed that a global maximum can be found. The practical computation uses a power iteration algorithm to find a local maximum and thus obtains a lower bound for μ. On the other hand, the calculation of an upper bound from (1.6) is a convex minimization problem for the maximal singular value, so all local minima are global. Hence, this bound is computationally attractive. In this research, we will initially use the commercially available MATLAB μ-toolbox to compute μ upper and lower bounds [4].

1.4 Linear fractional transformation

Linear fractional transformation (LFT) is an important concept when forming the standard μ analysis framework. It is defined as follows. Consider a matrix $M \in C^{n \times n}$ partitioned as

$$M = \begin{bmatrix} M_{11} & M_{12} \\ M_{21} & M_{22} \end{bmatrix} \tag{1.7}$$

with $M_{11} \in C^{n_1 \times n_1}$, $M_{22} \in C^{n_2 \times n_2}$ and $n_1 + n_2 = n$. Suppose we have block structures χ_{κ_1} and χ_{κ_2} defined as follows:

$$\begin{aligned} \chi_{\kappa_1} &= \left\{\Delta : \Delta \in C^{n_1 \times n_1}\right\} \\ \chi_{\kappa_2} &= \left\{\Delta : \Delta \in C^{n_2 \times n_2}\right\} \end{aligned}$$

then the block structure of χ_{κ} is defined as

$$\chi_\kappa := \left\{\Delta = \text{block diag}\left(\Delta_1, \Delta_2\right) : \Delta_1 \in \chi_{\kappa_1}, \Delta_2 \in \chi_{\kappa_2}\right\} \tag{1.8}$$

and is compatible with M. Now given any $\Delta_1 \in \chi_{\kappa_1}$, the LFT $F_u\left(M, \Delta_1\right)$ is said to be well-posed if and only if there exists a unique solution to the loop equations shown in Figure 1.1, namely

$$\begin{aligned} w &= M_{11} z + M_{12} d \\ e &= M_{21} z + M_{22} d \\ z &= \Delta_1 w \end{aligned}$$

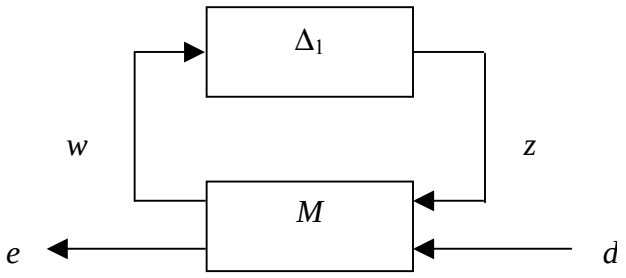

Figure 1.1 Upper LFT

It is easy to see that $F_u\left(M, \Delta_1\right)$ is well posed if and only if $\left(I_{n_1} - M_{11}\Delta_1\right)$ is invertible. When the LFT is well-posed, it is defined to be an unique mapping from d to e; i.e., the vectors e and d satisfy $e := F_u\left(M, \Delta_1\right)d$ where

$$F_u\left(M, \Delta_1\right) = M_{22} + M_{21}\Delta_1\left(I_{n_1} - M_{11}\Delta_1\right)^{-1} M_{12} \tag{1.9}$$

Note that in the above derivation we always assume that the feedback is closed around the top inputs and outputs, and hence we obtain an upper LFT (denoted by F_u). We can analogously define lower LFT (denoted by F_l) as

$$F_l\left(M, \Delta_2\right) = M_{11} + M_{12}\Delta_{12}\left(I_{n_2} - M_{22}\Delta_2\right)^{-1} M_{21} \tag{1.10}$$

A fundamental property of the LFT is that the interconnections of LFTs are again LFTs. Therefore, the LFT is very flexible in representing both parametric uncertainty and unmodeled dynamics.

1.5 Robust stability and the frequency sweep method

The general definition of μ is now extended to the linear system case. Instead of being a constant complex matrix, M is now a transfer function matrix. The following theorem addresses the robust stability of linear systems and gives rise to the most common usage of μ as a frequency domain robustness test.

Let $\mathrm{M}(\chi_\kappa)$ denote the set of all block diagonal and stable rational transfer functions that have a block diagonal structure such as χ_κ. And for $\Delta \in \mathrm{M}(\chi_\kappa)$, define $\|\Delta\|_\infty = \sup_\omega \bar{\sigma}\{\Delta(j\omega)\}$.

Theorem (Robust Stability [7]): Suppose $M(s)$ is a nominal stable system(otherwise the problem is trivial), then for all $\Delta \in \mathrm{M}(\chi_\kappa)$ with $\|\Delta\|_\infty < \frac{1}{\beta}$, the perturbed closed-loop system is well posed and internally stable if and only if

$$\sup_{\omega \in R} \mu_\kappa(M(j\omega)) < \beta \tag{1.11}$$

This theorem means that we can evaluate the robustness properties of a closed-loop system by using a frequency evaluation of μ. For any given frequency point we have a constant matrix μ problem, and the peak value of the frequency μ-plot determines the maximal size of the uncertainty for which the closed-loop system can maintain stability.

As mentioned above, the μ-toolbox software does not compute μ exactly, but bounds it from above and below by several optimization steps. Hence, the conclusion can be restated in terms of upper and lower bounds. If we let β_u and β_l be upper and lower bounds of μ respectively, then we can expect the following rules:

- For all uncertainty matrices Δ in $\mathrm{M}(\chi_\kappa)$ satisfying $\|\Delta\|_\infty < \frac{1}{\beta_u}$, the closed-loop system is stable;
- There is a particular uncertainty matrix Δ in $\mathrm{M}(\chi_\kappa)$ satisfying $\|\Delta\|_\infty = \frac{1}{\beta_l}$ that causes instability.

The restatement of the theorem suggests the need to search for max $\max_{i=1,\ldots,n} \bar{\mu}_\kappa(M(j\omega_i))$ and $\max_{i=1,\ldots,n} \underline{\mu}_\kappa(M(j\omega_i))$ instead of $\sup_{\omega \in R} \mu_\kappa(M(j\omega))$. This search involves a fairly large amount of computation. In practice a decision has to be made on the appropriate frequency range and the fineness of the grid. Thus there is possibility of missing important points. Moreover, in general, μ may be discontinuous so that the use of frequency sweeps may be misleading.

2 Power System Modeling

To perform robust analysis on a power system, we need to set up the required framework. First, the nominal system model must be obtained. Power system models are described in detail in the following sections. The synchronous generators are represented by a classical model (see chapter 2 of [9]) or two-axis model (see chapter 4 of [9]), with an excitation system represented by a ETMSP Type-30 model [10], and the power system stabilizer in a ETMSP Type-11 model [10]. The network is represented by steady-state network parameters with a constant impedance load model. By assuming that the generator internal reactance is constant, the network representation can be reduced to generator internal buses. The equations representing the various power system components can be coupled with the reduced network equations through a reference frame transformation. As a result, we obtained a set of coupled differential algebraic equations in the following form:

$$\begin{aligned} \dot{X} &= f(X, Z, u) \\ 0 &= g(X, Z) \end{aligned} \tag{2.1}$$

where X is the vector of state variables governed by the differential equations, and Z is the vector of network variables.

The procedure for obtaining a linearized model of the system given in (2.1) is summarized as follows. A power flow solution is obtained for a given operating condition, specified in terms of real and reactive power load, real power generation schedules at generator buses, and voltage magnitudes at certain buses. This solution provides the voltage magnitudes and angles at all the buses. With the voltage solution and the power injection at each generator bus, initial conditions for the state variables are calculated. The state equations and the network equations are then linearized, and a set of state-space equations representing the power system are obtained in the following form:

$$\begin{aligned} \dot{X}_\Delta &= AX_\Delta + FZ_\Delta \\ GX_\Delta &= HX_\Delta \end{aligned} \tag{2.2}$$

where X_Δ is the vector of incremental state variables; Z_Δ is the vector of incremental network variables; and A, F, G and H are coefficient matrices with proper dimensions. Chapter 3 in [11] schematically describes the structure of the coupled equations.

2.1 Generator model

In this project, we use two kinds of generator models: the two-axis model and the classical model [9]. We assume that in a power system with n-generators, the first m generators are represented by the two-axis model and are equipped with exciters, and the remaining (n-m) generators are represented by the classical model.

2.1.1 Classical model

The classical model is the simplest model to represent generators without excitation control in a multi-machine system (see Chapter 2 of [9]). It is based on the following assumptions:

1. Mechanical power input is constant;
2. Damping or asynchronous power is negligible;
3. Constant-voltage-behind-transient-reactance model for the synchronous machines is valid; and
4. The mechanical rotor angle of a machine coincides with the angle of the voltage behind the transient reactance.

With the loads represented by constant impedance, the load nodes and the terminal voltage nodes of the generators are eliminated. The resulting network contains only the internal generator nodes (numbered from 1 to *n*). The generator reactance and the constant impedance loads are included in the bus admittance matrix Y_{bus} of the reduced network.

The dynamic equations for the classical model are given by

$$M_i \dot{\omega}_i = P_i - P_{ei} \tag{2.3}$$

$$\dot{\delta}_i = \omega_i - \omega_s \qquad i = m+1, m = 2, \ldots, n \tag{2.4}$$

where

$$P_i = P_{mi} - E_i^2 G_{ii}$$

$$P_{ei} = \sum_{j=1, j\neq i}^{n} \left[E_i E_j B_{ij} \sin\left(\delta_i - \delta_j\right) + E_i E_j G_{ij} \cos\left(\delta_i - \delta_j\right) \right]$$

and

E_i: internal bus voltage of generator *i*

M_i: inertia constant of generator *i*

P_{mi}: mechanical power input of generator *i*

G_{ii}: driving point conductance of node *i*

$G_{ij} + B_{ij}$: the transfer admittance between node i and node j in the reduced network

ω_i : rotor speed of generator *i*(with respect to the synchronous frame)

ω_s : synchronous speed

δ_i : rotor angle of generator *i*

2.1.2 Two-axis model

Generators with excitation control are described by the two-axis model (see chapter 4 of [9]) in this report. The two-axis model accounts for the transient effects and requires the following assumptions.

1. In the stator voltage equations, the variation of flux linkages of d-q axes are negligible compared to the speed voltage terms.
2. $\omega \cong \omega_s = 1$ p.u.

The resultant dynamic equations are given by

$$\tau'_{doi}\dot{E}'_{qi} = E_{FDi} - E'_{qi} + \left(x_{di} - x'_{di}\right)I_{di} \tag{2.5}$$

$$\tau'_{qoi}\dot{E}'_{di} = -E'_{di} - \left(x_{qi} - x'_{qi}\right)I_{qi} \tag{2.6}$$

$$M_i\dot{\omega}_i = P_{mi} - \left(I_{di}E'_{di} + I_{qi}E'_{qi}\right) + \left(x'_{qi} - x'_{di}\right)I_{qi}I_{di} - \frac{D_i}{\omega_s}\left(\omega_i - \omega_s\right) \tag{2.7}$$

$$\dot{\delta}_i = \omega_i - \omega_s \qquad\qquad i = 1,2\ldots,m \tag{2.8}$$

where

E'_d, E'_q : direct and quadrature axes stator EMFs corresponding to rotor transient flux components, respectively

I_d, I_q : the d and q axes stator currents

τ'_{do}, τ'_{qo} : open-circuit direct and quadrature axes transient time constants

x_d, x'_d : direct axis synchronous and transient reactances

x_q, x'_q : quadrature axis synchronous and transient reactances

E_{FD} : stator EMF corresponding to the field voltage

D_i : damping coefficient of generator *i*.

2.1.3 Angle reference

In (2.4) and (2.8), we used the absolute rotor angles (δ_i , i = 1; 2; : : : ; n) as state variables. Since these n state variables are not independent, we can introduce the relative rotor angles as new state variables which are independent. Without loss of generality, δ_1 is chosen as a reference; then, the relative rotor angles are defined as:

$$\delta_{i1} = \delta_i - \delta_1, \qquad i = 2,3,\ldots,\mathrm{n}$$

The dynamic equations (2.3) --- (2.8) remain unchanged with each δ_i replaced by δ_{i1} and ω_s replaced by ω_1. Therefore, (2.4) and (2.8) become

$$\dot{\delta}_{i1} = \omega_i - \omega_1 \qquad i = 2,3,\ldots,n \tag{2.9}$$

2.2 Excitation system model

The type of excitation system used is the ETMSP Type-30 [10] (same as IEEE AC-4, see [12]) as shown in Figure 2.1. The state variables are E_{FD}, X_{E1}, and X_{E2}, and the dynamic equations are given by

$$\dot{E}_{FDi} = \frac{K_{Ai}}{T_{Ai}} X_{E2i} - \frac{1}{T_{Ai}} E_{FDi} + \frac{aK_{Ai}}{T_{Ai}} \left(V_{REFi} + V_{PSSi} - X_{E1i}\right) \tag{2.10}$$

$$\dot{X}_{E1i} = -\frac{1}{T_{Ri}} X_{E1i} + \frac{1}{T_{Ri}} V_{Ti} \tag{2.11}$$

$$\dot{X}_{E2i} = -\frac{1}{T_{Bi}} X_{E2i} + \frac{1-a}{T_{Bi}} \left(V_{REFi} + V_{PSSi} - X_{E1i}\right) \tag{2.12}$$

$$\begin{aligned} V_{Ti} &= V_{Tqi} + jV_{Tdi} \\ &= \left(E'_{qi} + x'_{di} I_{di}\right) + j\left(E'_{di} - x'_{qi} I_{qi}\right) \qquad i = 1,2,\ldots,n \end{aligned} \tag{2.13}$$

where

V_T : generator terminal voltage

V_{REF} : exciter reference voltage

V_{PSS} : power system stabilizer voltage

$a = T_{Ci}/T_{Bi}$, T_{Bi} and T_{Ci} are time constants

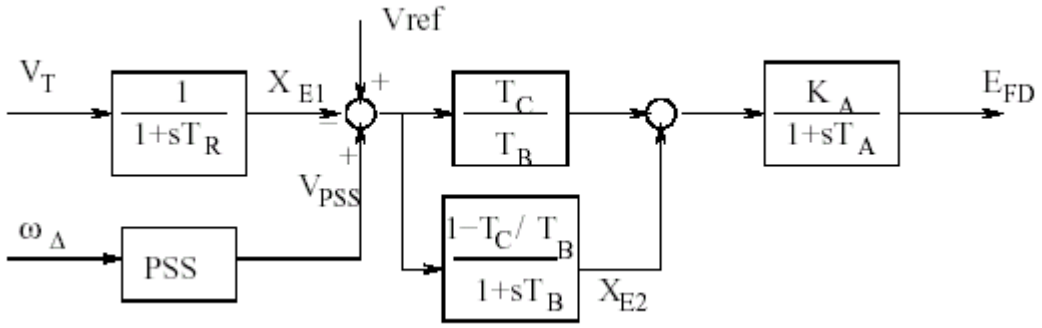

Figure 2.1 Excitation system model: ETMSP Type-30

2.3 Power system stabilizer model

A power system stabilizer (PSS) is used to add a modulation signal to a generator's voltage reference input. The idea is to produce an electric torque at the generator proportional to speed. Since there is a phase lag between the voltage signal and the electric torque, the PSS usually uses a simple phase lead compensator to adjust the input signal to give it the correct phase. Figure 2.2 shows the action of the PSS.

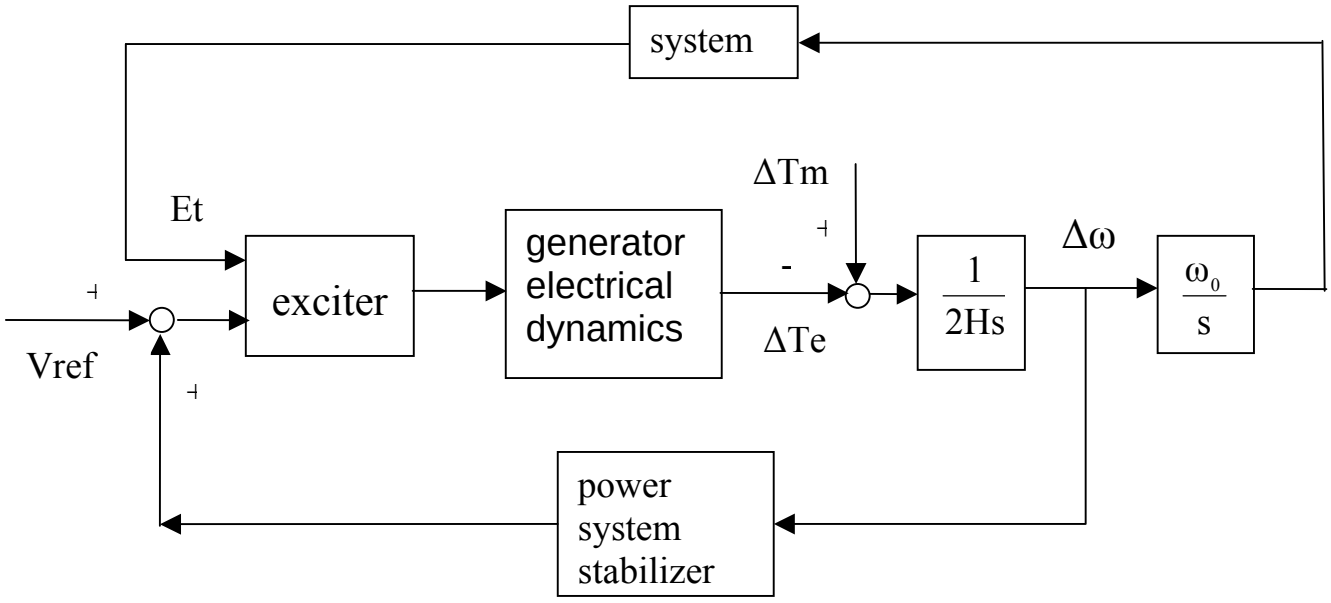

Figure 2.2 Block diagram showing stabilizer action

For performing the robustness analysis, a conventionally designed PSS is chosen. Its block diagram is shown in Figure 2.3. The state variables are, X_{S1}, X_{S2}, and X_{S3}. The equations for these variables are as follows:

$$\dot{X}_{S1i} = -\frac{1}{T_{5i}} X_{S1i} + \frac{1}{T_{5i}} K_{Si}\omega_{\Delta i} \tag{2.14}$$

$$\dot{X}_{S2i} = -\frac{1}{T_{2i}} X_{S2i} + \frac{1}{T_{2i}}\left(1 - \frac{T_{1i}}{T_{2i}}\right)\left[K_{Si}\omega_{\Delta i} - X_{S1i}\right] \tag{2.15}$$

$$\dot{X}_{S3i} = -\frac{1}{T_{4i}} X_{S3i} + \frac{1}{T_{4i}}\left(1 - \frac{T_{3i}}{T_{4i}}\right)\left[K_{Si}\omega_{\Delta i} - X_{S1i}\right] \tag{2.16}$$

$$V_{PSSi} = -\frac{T_{1i}T_{3i}}{T_{2i}T_{4i}} X_{S1i} + \frac{T_{3i}}{T_{4i}} X_{S2i} + X_{S3i} + \frac{T_{1i}T_{3i}}{T_{2i}T_{4i}} K_{Si}\omega_{\Delta i} \tag{2.17}$$

where $\omega_{\Delta_i} = \frac{\omega_i}{\omega_S} - 1$. When performing the linearization of the above equations,

$$\Delta\omega_{\Delta i} = \frac{\partial\omega_{\Delta i}}{\partial\omega_i}\Delta\omega_i = \frac{1}{\omega_S}\Delta\omega_i$$

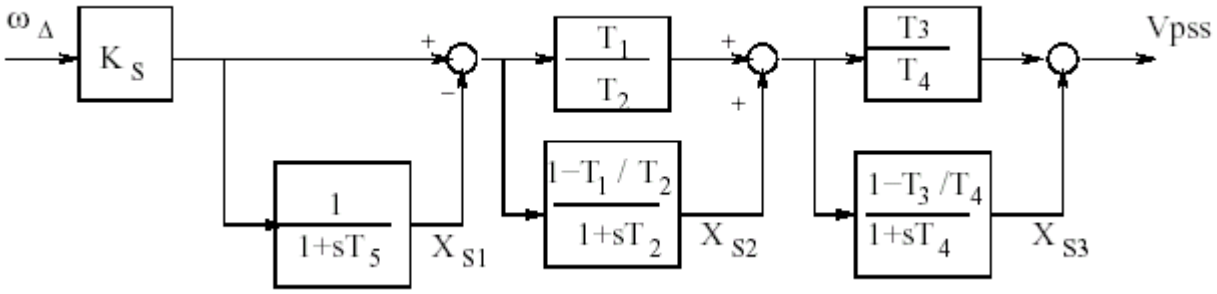

Figure 2.3 Power system stabilizer model

2.4 Network modeling

Constant impedance loads are used. By eliminating all the load nodes, the network is reduced to contain only the generator internal buses. The bus admittance matrix Y_{bus} consists of diagonal elements $Y_{ii}\angle\theta_{ii} = G_{ii} + jB_{ii}$, and off-diagonal elements $Y_{ij}\angle\theta_{ij} = G_{ij} + jB_{ij}$. Based on a procedure given in Chapter 9 of [9] the generator currents are given in the following form:

$$I_{qi} = \sum_{j=1}^{m}\left[F_{G+B}(\delta_{ij})E'_{qj} - F_{B-G}(\delta_{ij})E'_{dj}\right] + \sum_{k=m+1}^{n} F_{G+B}(\delta_{ik})E_k \tag{2.18}$$

$$I_{di} = \sum_{j=1}^{m}\left[F_{B-G}(\delta_{ij})E'_{qj} - F_{G+B}(\delta_{ij})E'_{dj}\right] + \sum_{k=m+1}^{n} F_{B-G}(\delta_{ik})E_k \tag{2.19}$$

$$I_k = \sum_{j=1}^{m} \left[F_{G+B}(\delta_{ij}) E'_{qj} - F_{B-G}(\delta_{ij}) E'_{dj} \right] + \sum_{l=m+1}^{n} F_{G+B}(\delta_{kl}) E_l \qquad (2.20)$$

$$i = 1,2,\ldots m \qquad k,l = m+1,\ldots,n$$

where

$$F_{G+B}(\delta_{ij}) = G_{ij} \cos(\delta_{ij}) + B_{ij} \sin(\delta_{ij}) \qquad (2.21)$$

$$F_{B-G}(\delta_{ij}) = B_{ij} \cos(\delta_{ij}) - G_{ij} \sin(\delta_{ij}) \qquad (2.22)$$

$$\delta_{ij} = \delta_i - \delta_j \qquad (2.23)$$

2.5 Overall system equation

The dynamic equations governing the generators, exciters, and the PSS have the following general form:

$$\dot{X} = f(X, Z, u) \qquad (2.24)$$

where

$X^T = \left[X_{SM}^T, X_{ES}^T, X_{PSS}^T \right]$, the vector of state variables

$X_{SM} = \left[E'_{q(1-m)}, E'_{d(1-m)}, \omega_{(1-n)}, \delta_{(2-n)1} \right]^T$

$X_{ES} = \left[E_{FD(1-m)}, X_{E1(1-m)}, X_{E2(1-m)} \right]^T$

$X_{PSS} = \left[X_{S1(1-m)}, X_{S2(1-m)}, X_{S3(1-m)} \right]^T$

$Z = \left[I_{q(1-m)}, I_{d(1-m)}, I_{[(m+1)-n]}, V_{T(1-n)} \right]^T$, the vector of network variables

$u = \left[V_{REF(1-m)} \right]^T$, the vector of control inputs

and **f** is the vector of nonlinear functions summarized below:

$$\begin{aligned} f_{1i} &= \dot{E}'_{qi} \qquad i = 1,\ldots,m \\ &= \frac{1}{\tau'_{doi}} \left[E_{FDi} - E'_{qi} + (x_{di} - x'_{di}) I_{di} \right] \end{aligned} \qquad (2.25)$$

$$f_{2i} = \dot{E}'_{di} \qquad i = 1,\ldots,m$$
$$= \frac{1}{\tau'_{qoi}}\left[-E'_{di} - \left(x_{qi} - x'_{qi}\right)I_{qi}\right] \tag{2.26}$$

$$f_{3i} = \dot{\omega}_i \qquad i = 1,\ldots,n$$
$$= \frac{1}{M_i}\left[P_{mi} - \left(I_{di}E'_{di} + I_{qi}E'_{qi}\right) + \left(x'_{qi} - x'_{di}\right)I_{qi}I_{di} - \frac{D_i}{\omega_s}\left(\omega_i - \omega_s\right)\right] \tag{2.27}$$

$$f_{4i} = \dot{\delta}_{i1} \qquad i = 1,\ldots,n$$
$$= \omega_i - \omega_1 \tag{2.28}$$

$$f_{5i} = \dot{E}_{FDi} \qquad i = 1,\ldots,m$$
$$= \frac{K_{Ai}}{T_{Ai}}X_{E2i} - \frac{1}{T_{Ai}}E_{FD_i} + \frac{aK_{Ai}}{T_{Ai}}\left(V_{REFi} + V_{PSSi} - X_{E1i}\right) \tag{2.29}$$

$$f_{6i} = \dot{X}_{E1i} \qquad i = 1,\ldots,m$$
$$= -\frac{1}{T_{Ri}}X_{E1i} + \frac{1}{T_{Ri}}V_{Ti} \tag{2.30}$$

$$f_{7i} = \dot{X}_{E2i} \qquad i = 1,\ldots,m$$
$$= -\frac{1}{T_{Bi}}X_{E2i} + \frac{1-a}{T_{Bi}}\left(V_{REFi} + V_{PSSi} - X_{E1i}\right) \tag{2.31}$$

$$f_{8i} = \dot{X}_{S1i} \qquad i = 1,\ldots,m$$
$$= -\frac{1}{T_{5i}}X_{S1i} + \frac{1}{T_{5i}}\frac{K_{Si}}{\omega_S}\Delta\omega_i \tag{2.32}$$

$$f_{9i} = \dot{X}_{S2i} \qquad i = 1,\ldots,m$$
$$= -\frac{1}{T_{2i}}X_{S2i} + \frac{1}{T_{2i}}\left(1 - \frac{T_{1i}}{T_{2i}}\right)\left[\frac{K_{Si}}{\omega_S}\Delta\omega_i - X_{S1i}\right] \tag{2.33}$$

$$f_{10i} = \dot{X}_{S3i} \qquad i = 1,\ldots,m$$
$$= -\frac{1}{T_{4i}}X_{S3i} + \frac{1}{T_{4i}}\left(1 - \frac{T_{3i}}{T_{4i}}\right)\left[X_{S2i} + \frac{T_{1i}}{T_{2i}}\left(\frac{K_{Si}}{\omega_S}\Delta\omega_i - X_{S1i}\right)\right] \tag{2.34}$$

Note that we use (2.27) to model generators in the two-axis model as well as in the classical model. This is true because the classical model can be viewed as a special case of the two-axis model with $E_q^{'} = E, E_d^{'} = 0, I_q = I,$ and $I_d = 0.$

Linearization of (2.24) leads to

$$\Delta \dot{X} = \frac{\partial f}{\partial X}\Delta X + \frac{\partial f}{\partial Z}\Delta Z + \frac{\partial f}{\partial u}\Delta u \tag{2.35}$$

We also have the network algebraic equation

$$0 = g(X, Z) \tag{2.36}$$

This equation is linearized and organized so that all the terms related to the algebraic variables are put on one side of the equation and those related to the state variables are on the other side of the equation.

We obtain the representation of the whole system in the state space form as

$$\Delta \dot{X} = A\Delta X + F\Delta Z + B\Delta u \tag{2.37}$$

$$G\Delta Z = H\Delta X \tag{2.38}$$

where

$$A = \frac{\partial f}{\partial X}, F = \frac{\partial f}{\partial Z}, B = \frac{\partial f}{\partial u} \tag{2.39}$$

The procedure to obtain *G*, *H* and the detailed expressions for the elements of all the coefficient matrices are given in [30].

2.6 Uncertainty characterization

As mentioned in the introduction to Section 2, the state-space representation will be used to capture the parameter uncertainties in the system matrices. In [3], the parameter uncertainties in the system equations were characterized in the differential equations that were obtained after representing all the network variables by the state variables. A more natural way of characterizing the uncertainties was investigated in this project, where the uncertainties in the algebraic equations and differential equations were considered separately.

In this project, the uncertainties were different operating conditions in the power system, which are represented by parameter variation such as in tie-line power flow, total generation of certain areas, etc. When the operating condition changes, some elements of the coefficient matrices of the dynamic equation (2.2) also change. Our analysis shows that the dependence of such a change on the parameter variation can be approximated by a low order polynomial. Results show

that linear approximation achieves very good accuracy as compared to quadratic approximations in [3].

Next, we cast our problem as a robust stability problem in the canonical $M-\Delta$ framework to apply the SSV method. The range of the operating parameters within which the system can remain stable is determined. For simplicity, we only took one operating parameter *p* varying within the known interval $[\,p^{\min}, p^{\max}\,]$. Two or more varying parameters can be treated in a similar way. Those coefficients of the matrices in the dynamic equation (2.2) that depend on *p* will change with the change of operating conditions. Consider the entries of the *A*-matrix as an example. Each element of the *A*-matrix in (2.2) that depends on the parameter can be expressed as follows:

$$a_{ij} = a'_{ij0} + a'_{ij1} p \tag{2.40}$$

It is desirable to normalize the range of uncertain parameter to the interval [-1,1]. Let

$$p = \frac{p^{\max} + p^{\min}}{2} + \frac{p^{\max} - p^{\min}}{2}\delta \tag{2.41}$$

where $-1 \le \delta \le 1$. Note that as δ varies within the interval-1; 1], *p* will vary within the interval $\left\lfloor p^{\min}, p^{\max} \right\rfloor$. Thus, the variation in *p* is captured by the variation in δ. When (2.41) is substituted into (2.40), we get a_{ij} as a polynomial of δ. Then (2.40) can be rewritten as:

$$a_{ij} = a_{ij0} + a_{ij1}\delta \tag{2.42}$$

where δ takes the values in the interval [-1,1], and a_{ijk} depends on a'_{ijk}, $p^{\min}$, and $p^{\max}$.

Based on the above representation, it is possible to write the system equations with one perturbed real parameter as follows:

$$\begin{aligned} \dot{X} &= (A_0 + \delta A_1)X + (F_0 + \delta F_1)Z \\ (G_0 + \delta G_1)Z &= (H_0 + \delta H_1)X \end{aligned} \tag{2.43}$$

where $\delta \in [-1,+1]$; $A_0 = \lfloor a_{ij0} \rfloor$ is the matrix of the constant part in equation (2.40), and $A_1 = \lfloor a_{ij1} \rfloor$ is the matrix of the coefficients of the first order part in equation (2.40); F_0, G_0, H_0 are matrices of the constant parts after linear curve-fitting for *F*, *G*, *H* respectively while F_1, G_1 and H_1 are the respective first order part. Note that we omitted the subscript Δ, and that all the variables are actually incremental. Since G_0 is invertible (see expression for G_0 in [30]), we can rewrite the above equations as follows:

$$\begin{bmatrix} \dot{X} \\ Z \end{bmatrix} = \begin{bmatrix} A_0 & F_0 \\ G_0^{-1}H_0 & 0 \end{bmatrix} \begin{bmatrix} X \\ Z \end{bmatrix} + \delta \begin{bmatrix} A_1 & F_1 \\ G_0^{-1}H_1 & -G_0^{-1}G_1 \end{bmatrix} \begin{bmatrix} X \\ Z \end{bmatrix} = P \begin{bmatrix} X \\ Z \end{bmatrix} + \delta R \begin{bmatrix} X \\ Z \end{bmatrix} \tag{2.44}$$

where the matrices P and R are defined by

$$P = \begin{bmatrix} A_0 & F_0 \\ G_0^{-1}H_0 & 0 \end{bmatrix} \tag{2.45}$$

$$R = \begin{bmatrix} A_1 & F_1 \\ G_0^{-1}H_1 & G_0^{-1}G_1 \end{bmatrix} \tag{2.46}$$

Singular Value Decomposition (SVD) is then used to reduce the order of the system. By using SVD factorization for R, we have

$$R = U \sum V^H$$

The matrix Σ is diagonal with the singular values in decreasing order on the diagonal. The matrices U and V are unitary matrices and the superscript H denotes the Hermitian conjugate, which equals the normal transpose in the case of real matrices. The matrix R has precisely $r = rank(R)$ number of singular values that are separated from zero. If we partition the matrix U and V according to the non-zero singular values, we get

$$R = \begin{bmatrix} U_1 & U_2 \end{bmatrix} \begin{bmatrix} \Sigma_r & 0 \\ 0 & 0 \end{bmatrix} \begin{bmatrix} V_1 & V_2 \end{bmatrix}^H = U_1 \Sigma_r V_1^H \tag{2.47}$$

Now we let $R_1 = U_1$ and $R_2 = \Sigma_r V_1^H$. This allows us the possibility of reducing the order of the system.

To extract the uncertainty δ, we define the vectors v and w as

$$v = R_2 \begin{bmatrix} X \\ Z \end{bmatrix} \tag{2.48}$$

$$w = \delta v \tag{2.49}$$

Due to the factorization, the size of the vectors v and w will be exactly $r = rank(R)$. If R is of low rank, then the order of the uncertainty block will be reduced significantly. Now,

$$\begin{bmatrix} \dot{X} \\ Z \end{bmatrix} = P\begin{bmatrix} X \\ Z \end{bmatrix} + R_1\delta v = P\begin{bmatrix} X \\ Z \end{bmatrix} + R_1 w = P\begin{bmatrix} X \\ Z \end{bmatrix} + R_1\begin{bmatrix} w_{\dot{X}} \\ w_Z \end{bmatrix} \tag{2.50}$$

Adding v to the outputs and w to the inputs we get

$$\begin{bmatrix} v \\ \begin{bmatrix} \dot{X} \\ Z \end{bmatrix} \end{bmatrix} = \begin{bmatrix} 0 & R_2 \\ R_1 & P \end{bmatrix}\begin{bmatrix} w \\ \begin{bmatrix} X \\ Z \end{bmatrix} \end{bmatrix} \tag{2.51}$$

Partition R_1, R_2, P, as follows:

$$R_2 = \begin{bmatrix} R_{2,X} & R_{2,Z} \end{bmatrix} \tag{2.52}$$

$$R_1 = \begin{bmatrix} R_{1,\dot{X}} \\ R_{1,Z} \end{bmatrix} \tag{2.53}$$

$$P = \begin{bmatrix} P_{\dot{X},X} & P_{\dot{X},Z} \\ P_{Z,X} & P_{Z,Z} \end{bmatrix} \tag{2.54}$$

Then,

$$\begin{bmatrix} v \\ \begin{bmatrix} \dot{X} \\ Z \end{bmatrix} \end{bmatrix} = \begin{bmatrix} 0 & R_{2,X} & R_{2,Z} \\ R_{1,\dot{X}} & P_{\dot{X},X} & P_{\dot{X},Z} \\ R_{1,Z} & P_{Z,X} & P_{Z,Z} \end{bmatrix}\begin{bmatrix} w \\ \begin{bmatrix} X \\ Z \end{bmatrix} \end{bmatrix} \tag{2.55}$$

Rearranging the input and output, we get

$$\begin{bmatrix} Z \\ \begin{bmatrix} \dot{X} \\ v \end{bmatrix} \end{bmatrix} = \begin{bmatrix} P_{Z,Z} & P_{Z,X} & R_{1,Z} \\ P_{\dot{X},Z} & P_{\dot{X},X} & R_{1,\dot{X}} \\ R_{2,Z} & R_{2,X} & 0 \end{bmatrix}\begin{bmatrix} Z \\ \begin{bmatrix} X \\ w \end{bmatrix} \end{bmatrix} \tag{2.56}$$

Taking Z as the internal signal,

$$\begin{bmatrix} \dot{X} \\ v \end{bmatrix} = \mathrm{T}\begin{bmatrix} X \\ w \end{bmatrix} \tag{2.57}$$

where

$$\mathrm{T} = \begin{bmatrix} P_{\dot{X},X} & R_{1,\dot{X}} \\ R_{2,X} & 0 \end{bmatrix} + \begin{bmatrix} P_{\dot{X},Z} \\ R_{2,Z} \end{bmatrix} \left(I - P_{Z,Z}\right)^{-1} \begin{bmatrix} P_{Z,X} & R_{1,Z} \end{bmatrix} \qquad (2.58)$$

This process of "pulling out"' and isolating the uncertainty to get the resulting interconnection of known system components and uncertain parameters is redrawn in Figure 2.4, where *M* is a known dynamic system and Δ is a diagonal (structured) perturbation which accounts for the uncertainty.

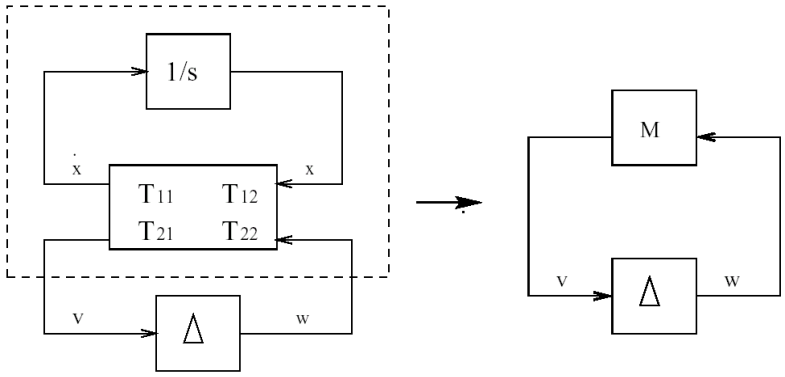

Figure 2.4 Robust stability analysis framework

The uncertainty characterization adopted in this project captures the uncertainty in the network components in a more direct fashion than has been done before when the network algebraic equations were reduced to obtain a system of differential equations to represent the system.

2.7 Numerical results to verify uncertainty characterization

The robustness analysis approach was first applied to a four-machine, two-area sample system, as shown in Figure 2.5. This system was specially designed by Ontario Hydro to study the fundamental nature of inter-area oscillations [13].

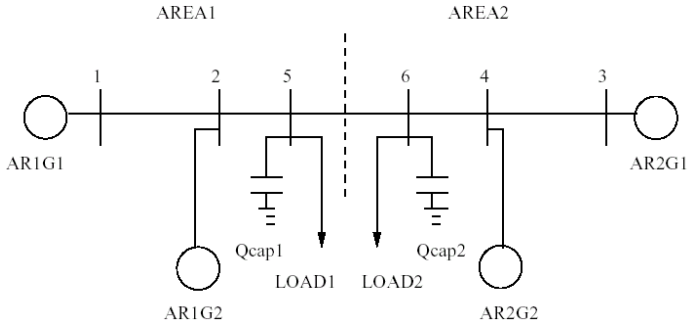

Figure 2.5 Four-machine two-area test system

For the 4-machine, 2-area test system, the exporting power from Area 1 was chosen as the uncertainty, which was allowed to vary in the range [0 - 400] MW. Load 1 was varied in the range [1140 - 1540] MW while Load 2 was varied in the range [1400 -1800] MW.

Using the given value of the control parameters, robustness analysis was done using the proposed uncertainty formulation. The μ results were evaluated for the given range of varying parameters. The results for the proposed formulation are shown in Table 2.1 under the symbol "DAE". The estimated exporting power was obtained by repeatedly performing the eigenvalue test, while increasing the varying parameter (power export) to find the "critical" system eigenvalues. As a comparison, the robustness analysis results using the lumped differential equation (under symbol "DE") to capture uncertainties [3] are also listed.

Table 2.1 Robust Analysis Results for 4-Machine System

	DAE	DE
μ upper bound	1.4913	1.4550
Estimated P_{exp} (MW)	334.1	337.5
Exact exporting power (MW)	344.5	344.5
Error (%)	3.02	2.04
Size of Δ	14	22

From Table 2.1 we see that using linear approximation in the proposed approach for uncertainty characterization can achieve accuracy comparable with that achieved by using quadratic approximation in the "DE" method. The uncertainty characterization does not overbound the uncertainty and provides stability results that compare well with the repeated calculation using eigenvalue analysis.

Another test was performed on a fifty-machine system [14]. This is a moderate-sized system which includes all the modeling features and the complexity of large-scale power systems. A one-line diagram of the area of interest is shown in Figure 2.6.

This test system contains 44 generators represented by the classical model with uniform damping and 6 generators represented by a two-axis model. All classical modeled machines have uniform damping $D_i/M_i = 0{:}1$ except machines at buses #137 and #140 which have $D_i/M_i = 0{:}5$. The base case power flow was characterized by setting the generation at Bus #93 and #110 to be 1250MW. This generation was treated as uncertain and was allowed to vary in the range [2*1150-2*1350] MW.

By performing an eigenvalue test, the exact critical generation was obtained as 1320.5MW. The robust analysis results using the differential algebraic model with the changing elements in the A matrix represented by linear approximation are shown in Table 2.2. Note that the peak of μ-plot in both cases was larger than 1.0 so the robust stability was not achieved within the given operating range. In both cases, the estimated stability limits agreed with the exact stability limits. Therefore, we can conclude that the proposed method provides a precise tool for the evaluation of power system robust stability.

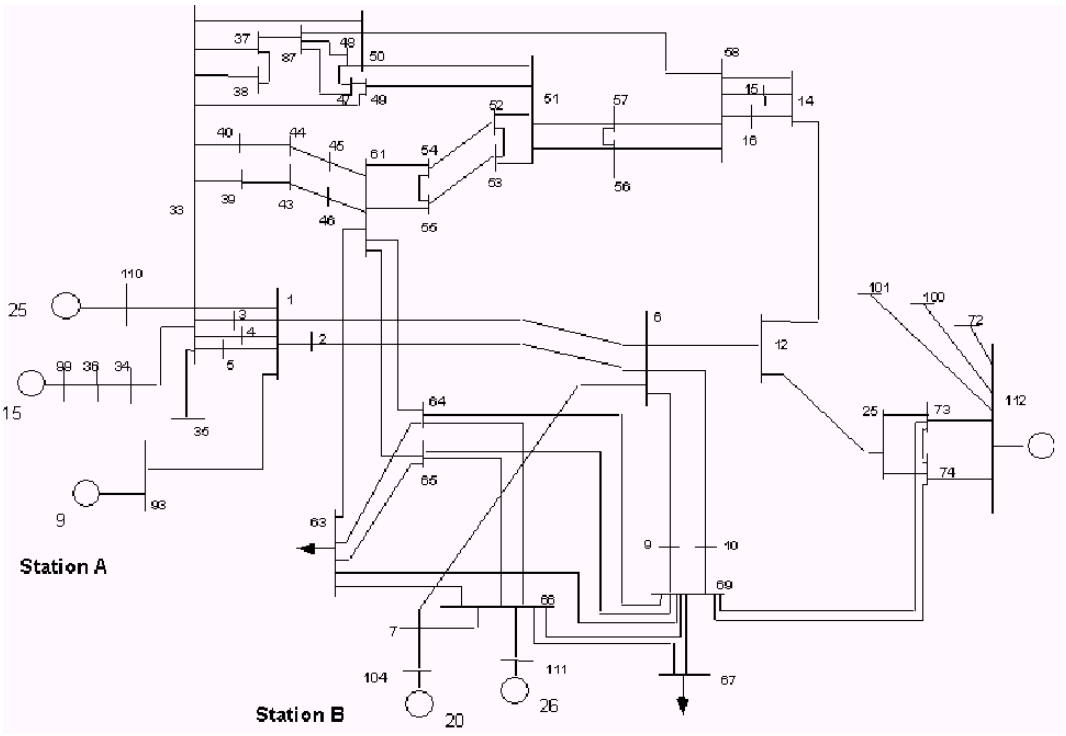

Figure 2.6 IEEE 50-generator system: a one-line diagram of the study area

Table 2.2 Robust Analysis Results for 50-Machine System

	DAE	DE
μ upper bound	1.4217	1.4436
Estimated critical generation (MW)	1320.3	1319.3
Exact critical generation (MW)	1320.5	1320.5
Error (%)	1.5×10^{-4}	9.1×10^{-4}
Size of Δ	112	122

3 Reducing Computation Burden in the Evaluation of μ

In the preceding sections we have provided an introduction to the SSV or μ-based approach to analyze robust stability of power systems. The power system model has been formulated in the μ-framework, and a novel uncertainty characterization has been proposed. In this section we detail the approaches that have been taken to reduce the computational burden in evaluating μ. Three specific areas in μ- computation will be addressed. These relate to

- Frequency sweep,
- Calculation of lower bound of μ, and
- Calculation of upper bound of μ.

In each of these areas the steps taken to improve the efficiency of the μ-calculation will be clearly outlined. Tests conducted on a test power system model to determine the efficacy of the developed approaches will also be presented.

3.1 The state space test

The state space test method [6] for the analysis of robust stability can avoid the frequency sweep. The main idea is that a transfer function can be expressed as a linear fractional transformation (LFT) of a constant matrix with respect to the frequency variable, and the frequency variable can then be treated as an uncertainty so that the SSV technique can be applied directly.

Given a transfer function $M(s)$ in the M - Δ framework, we write it as an upper LFT:

$$M(s) = C(sI_p - A)^{-1}B + D = F_u\left(\begin{bmatrix} A & B \\ C & D \end{bmatrix}, \frac{1}{s} I_p\right) \tag{3.1}$$

where p is the dimension of the state space and $(A;B;C;D)$ is a state space realization of $M(s)$.

If we denote

$$M_f = \begin{bmatrix} A & B \\ C & D \end{bmatrix}$$

then the state equation for the robust stability problem of M - Δcan be written as

$$\dot{x} = F_l(M_f, \Delta)x \tag{3.2}$$

where $F_l(M_f, \Delta) = A + B\Delta(I - D\Delta)^{-1}C$. This is illustrated in Figure 3.1.

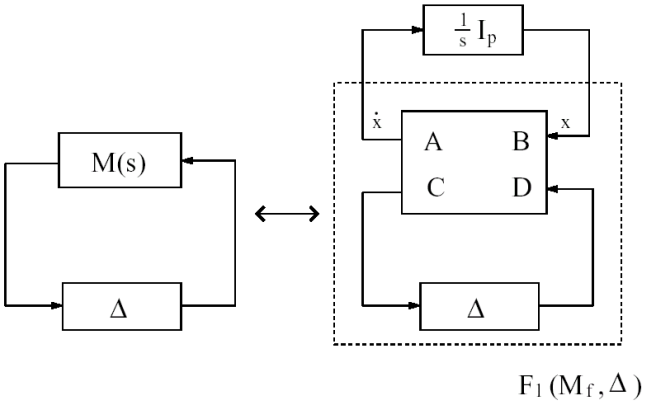

Figure 3.1 Transfer function in state space equation form with LFT

Next we want to remove the frequency search and include $\frac{1}{s} I_p$ as one of the uncertainties. Since μ usually considers uncertainty inside the unit disk, while $\frac{1}{s} I_p$ covers the right half of the *s*-plane, we may apply a bilinear transformation to map the right half of the *s*-plane into the unit disk on the complex plane (see Figure 3.2).

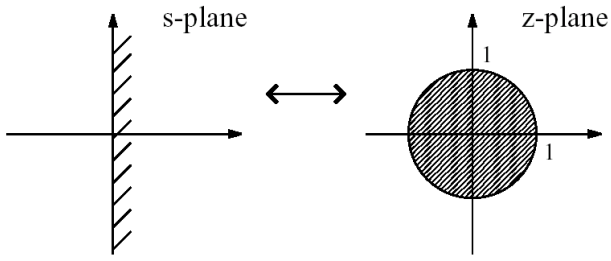

Figure 3.2 Bilinear Transformation: the right half of the *s*-plane to the unit disk in the *z*-plane

where

$$s = \frac{1-z}{1+z}, z \in C, |z| \le 1$$

and therefore,

$$\frac{1}{s} I_p = \frac{1+z}{1-z} I_p$$

This can be written in an LFT from again as:

$$\frac{1}{s} I_p = F_u\left(Q, zI_p\right) \text{where } Q = \begin{bmatrix} I_p & 2I_p \\ I_p & I_p \end{bmatrix}$$

Now we can replace $\frac{1}{s} I_p$ with the LFT of this constant matrix Q with respect to the new frequency variable z, as shown in Figure 3.3. The interconnection of Q and M_f in lower and upper LFT can be simplified using Redhaffer's star product [15]. This results in a new connection shown in Figure 3.3.c with matrix T in the following form:

$$T = \begin{bmatrix} I_p + 2A\left(I_p - A\right)^{-1} & 2\left(I_p - A\right)^{-1} B \\ C\left(I_p - A\right)^{-1} & D + C\left(I_p - A\right)^{-1} B \end{bmatrix}$$

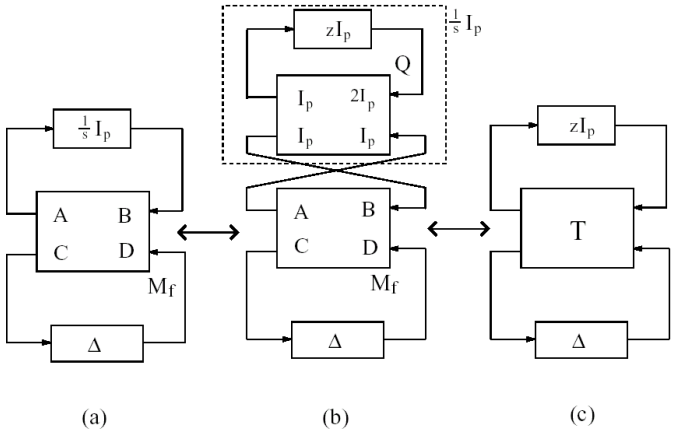

Figure 3.3 Frequency sweep transformed to state space test: A constant μ problem

From Figure 3.3, we eliminate the frequency sweep by including the frequency variable as one of the uncertainty parameters (a repeated complex scalar block). In this way, we obtain a one-shot μ test involving a constant matrix μ problem. This is formally stated in the following theorem:

Theorem (Robust stability with state space test) [7]

$$\sup_{\omega \in R} \mu_{\Delta}\left(M\left(j\omega\right)\right) \le 1 \quad \textit{if and only if} \quad \mu_{\widetilde{\Delta}}\left(T\right) \le 1$$

where $\widetilde{\Delta} = \left\{diag\left(zI_p, \Delta\right), z \in C, |z| \le 1\right\}$.

Note that this theorem only tells us whether $\sup_{\omega} \mu_{\Delta}(M(j\omega))$ is less than or equal to 1, which is a direct test for robust stability/instability. In order to compute the value of $\sup_{\omega} \mu_{\Delta}(M(j\omega))$, we need to define:

$$T_{\alpha} = \begin{bmatrix} T_{11} & \frac{1}{\alpha} T_{12} \\ T_{21} & \frac{1}{\alpha} T_{22} \end{bmatrix} \tag{3.3}$$

$$\tilde{\mu}(T) = \inf_{\alpha} \{\alpha \geq 0 : \mu_{\tilde{\Delta}}(T_{\alpha}) \leq 1\} \tag{3.4}$$

Then the above theorem can be restated as:

$$\sup_{\omega \in R} \mu_{\Delta}(M(j\omega)) = \tilde{\mu}(T) \tag{3.5}$$

Note that the right hand side of (3.4) involves a search over α; thus, we have not totally eliminated the need to search. Since $\mu_{\tilde{\Delta}}(T_{\alpha})$ is monotonically decreasing as α increases, the binary search can be used for (3.4) which involves only several constant μ calculations.

As mentioned before, the μ-toolbox software computes the lower and upper bounds instead of the exact value of μ. Therefore, we also obtain lower and upper bounds for $\tilde{\mu}(T)$. Since the upper and lower bounds of $\mu_{\tilde{\Delta}}(T_{\alpha})$ may not be always monotonic, a linear search over α is still needed.

3.2 Bounded frequency test

In light of the state space test, an alternative solution is proposed [16] to transform a classical frequency dependent μ analysis problem into a bounded frequency test problem in which the frequency ω is introduced as an additional uncertainty. Unlike the state space test, which treats the frequency variables over the whole frequency space (complex variables over the whole right half plane) as uncertainties, this test could obtain μ over a specified frequency range while the frequency is treated as a real scalar parameter.

Consider the interconnection structure $M(s)$-Δ, where Δ is the structured perturbation. We would like to compute without frequency gridding $\mu_{\max} = \max_{\omega \in [\omega_{\min}, \omega_{\max}]} \mu_{\kappa}(M(j\omega))$

In order to do this, we need to derive an LFT model for the dynamic system $M(j\omega)$ in which the frequency is viewed as a real scalar parameter. Let $(A;B;C;D)$ be the state-space model of the transfer function matrix $M(s)$. For a given positive ω, the matrix H satisfying $M(j\omega) = F_u(H, \omega I)$ is given as follows:

$$H = \begin{bmatrix} jA^{-1} & A^{-1}B \\ -jCA^{-1} & -CA^{-1}B + D \end{bmatrix} \tag{3.6}$$

To normalize the frequency uncertainty, let

$$\omega = \omega_0 + \omega_1 \times \delta\omega ,$$

where

$$\omega_0 = (\omega_{\max} + \omega_{\min})/2, \omega_1 = (\omega_{\max} - \omega_{\min})/2$$

we have

$$\begin{aligned} M(j\omega) &= D + C(j\omega I - A)^{-1} B \\ &= D + C[j(\omega_0 + \omega_1 \delta\omega) I - A]^{-1} B \\ &= D + C[j(\omega_1 \delta\omega) I - (A - j\omega_0 I)]^{-1} B \end{aligned}$$

Let

$$A' = A - j\omega_0 I, H(\omega_0) = \begin{bmatrix} jA'^{-1} & A'^{-1}B \\ -jCA'^{-1} & -CA'^{-1}B + D \end{bmatrix}$$

then

$$M(j\omega) = F_u(H(\omega_0), (\omega_1 \delta\omega) I)$$

Absorb ω_1 into H and let

$$H_1(\omega_0) = \begin{bmatrix} jA'^{-1}\omega_1 & A'^{-1}B \\ -jCA'^{-1}\omega_1 & -CA'^{-1}B + D \end{bmatrix}$$

We get the normalized perturbation blocks $\overline{\Delta}$ as: $\overline{\Delta} = \begin{bmatrix} \delta\omega I & 0 \\ 0 & \Delta \end{bmatrix}$. This process is shown in Figure 3.4.

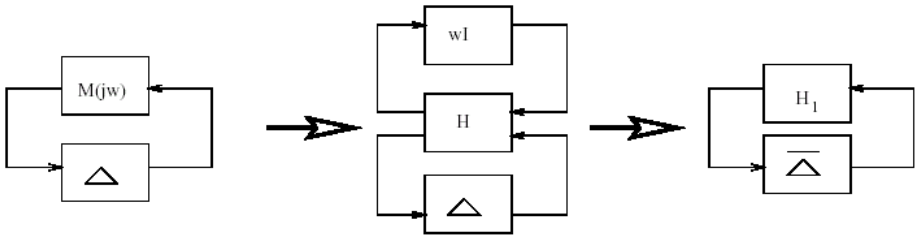

Figure 3.4 Formulation of the bounded frequency test

Theorem ([16]) With the notation introduced before,

$$\mu_{\max} = \max_{\omega\in[\omega_{\min},\omega_{\max}]} \mu_{\Delta}\left(M(j\omega)\right) \le 1 \text{ iff } \mu_{\overline{\Delta}}(H_1) \le 1 \qquad (3.7)$$

This theorem provides a reliable approach to check robust stability in the sense that the potential problems with frequency discontinuities are avoided. Now we can solve the robustness analysis problem on the $H_1(\omega_0) - \overline{\Delta}$ framework. In doing so, this bounded frequency test reduces our problem to a single constant μ problem with purely real uncertainties, thereby arriving at a very fast solution of the original problem.

Next, we need to perform a similar α searching process as in a state space test to find the maximum uncertainty size before instability occurs. The introduction of α factor is related to the concept of "skewed-μ" [15]. Skewed-μ is used when we need to check how large a particular source of uncertainty can be before the system loses stability while keeping other blocks fixed. If we have two uncertainties, say $\Delta = diag\{\Delta_1, \Delta_2\}$, and assume we have fixed $\|\Delta_1\| \le 1$, and we want to find how large Δ_2 can be before we get instability, then the solution is to shrink Δ_2 by a factor of α and find the smallest value of α which makes $\mu_{\overline{\Delta}}(H_1) \le 1$, where $\overline{\Delta} = diag\left\{\Delta_1, \frac{1}{\alpha}\Delta_2\right\}$. The above idea can be restated as follows:

Theorem

$$\max_{\omega} \mu_{\Delta}\left(M(j\omega)\right) = \inf_{\alpha}\left\{\alpha \,\middle|\, \mu_{\overline{\Delta}}\left(H_1'\right) \le 1\right\} \text{with } H_1' = \begin{bmatrix} H_{1_{11}} & \frac{1}{\alpha}H_{1_{12}} \\ H_{1_{21}} & \frac{1}{\alpha}H_{1_{22}} \end{bmatrix} \qquad (3.8)$$

Note that in this theorem, the shrinking factor α for the uncertainty block Δ has been absorbed into the system matrix $H_1(\omega_0)$ to form H_1'. It can be proved that $\mu_{\Delta}\left(H_1'\right)$ is a monotonically decreasing function of α, thus allowing a systematic way of finding α, such as by a bisection procedure.

A problem with this approach is that we have to use upper or lower bounds as substitutes for $\mu_{\Delta}(H_1')$ in the α searching procedure. Although the exact $\mu_{\Delta}(H_1')$ is a monotonically decreasing function with respect to α, its bounds are not necessarily monotonic. This is especially true of the lower bounds. Sometimes we only get poor lower bounds due to the non-convex nature of the problem. This leads to difficulty in applying the bisection algorithm. To compensate for this disadvantage, we propose to combine this test with branch and bound schemes. By doing this, we do not need to perform the α searching, and we can take advantage of the frequency sweep without worrying about missing important frequency points.

3.3 Branch and bound scheme

In this branch and bound scheme, the objective is to find the frequency where the $\sup_{\omega \in R} \mu_{\kappa}(M(j\omega))$ occurs. We first screen the frequency intervals using a bounded frequency test which is only a one-shot μ test at a certain frequency interval. After eliminating all the intervals with $\mu_{\bar{\Delta}}(H_1)$ less than 1, we perform a frequency sweep test on the remaining intervals. This provides an intelligent way to do a frequency sweep instead of blindly choosing the frequency interval to perform the sweep. The screening results of the branch and bound procedure give frequency ranges small enough to indicate where the instability might happen.

We use the upper bound information to determine whether a certain frequency interval should be thrown away. If the upper bound of $\mu_{\bar{\Delta}}(H_1)$ is less than 1, $\mu_{\bar{\Delta}}(H_1)$ it will definitely be less than 1. Such an interval can be eliminated. To perform faster screening, we try to use rough upper bounds whenever possible. For any $M \in C^{n\times n}, \mu_{\Delta}(M) \le \inf_{D\in D_{\kappa}} \bar{\sigma}(DMD^{-1})$ where D_{κ} is a set of matrices commutable with all the matrices in χ_{κ}, see equation (1.5) for details.

The branch and bound scheme for our problem will be as follows:

branch$[\omega_{\min}, \omega_{\max}]$
while $\omega_{\max} - \omega_{\min} > tolerance$
perform the bounded frequency test over $[\omega_{\min}, \omega_{\max}]$.

Let $U =$ *the upper bound of* $\mu_{\bar{\Delta}}(H_1)$;
if $U < 1$ *break* ;
else *branch*$[\omega_{\min}, (\omega_{\max} + \omega_{\min})/2]$;
branch$[(\omega_{\max} + \omega_{\min})/2, \omega_{\max}]$
endif
endwhile

3.4 Numerical results to verify efficacy of bounded frequency and branch and bound schemes

These tests were conducted for the 4-machine test system. The same operating conditions specified in Section 2.7 were used.

3.4.1 Bounded frequency test

- One Shot μ test

  A frequency range of [2:65; 2:85] r/s, which includes the critical frequency, was selected. The one shot μ test gave the upper bound of $\mu_{\bar{\Delta}}(H_1)$ as 1.9527 and the lower bound as 1.5346, which indicates that the exact $\mu_{\bar{\Delta}}(H_1)$ must be greater than 1. So we can conclude that the system is unstable within the given uncertainty range.

- Estimate the parameter range for a stable operation

  Figure 3.5 gives the upper and lower bounds of $\mu_{\bar{\Delta}}(H_1^{'})$ corresponding to the change in α. Since the upper bound remains above one, it provides no information on when the exact $\mu_{\bar{\Delta}}(H_1^{'})$ goes down through one. But if we look at the lower bound, when α = 1.35, the lower bound of $\mu_{\bar{\Delta}}(H_1^{'})$ is still above one. Thus, we can say that the exact $\mu_{\bar{\Delta}}(H_1^{'})$ goes down through one at least after α = 1.35. Since there is no point beyond α = 1.35 that gives the value of the lower bound of $\mu_{\bar{\Delta}}(H_1^{'})$ greater than one, we can use 1.35 as an approximation of $\tilde{\mu}$. Accordingly, we found the estimate value of the critical exporting power as 348 MW. Compared to the results from the eigenvalue test where the value of the critical exporting power was 344.5 MW, the error is only 0:2%.

These results indicate that the bounded frequency test shows promise and provides a stability limit that is quite close to the actual limit predicted by the repeated eigenvalue test. However, it still requires an α search to estimate the stable limit of operation

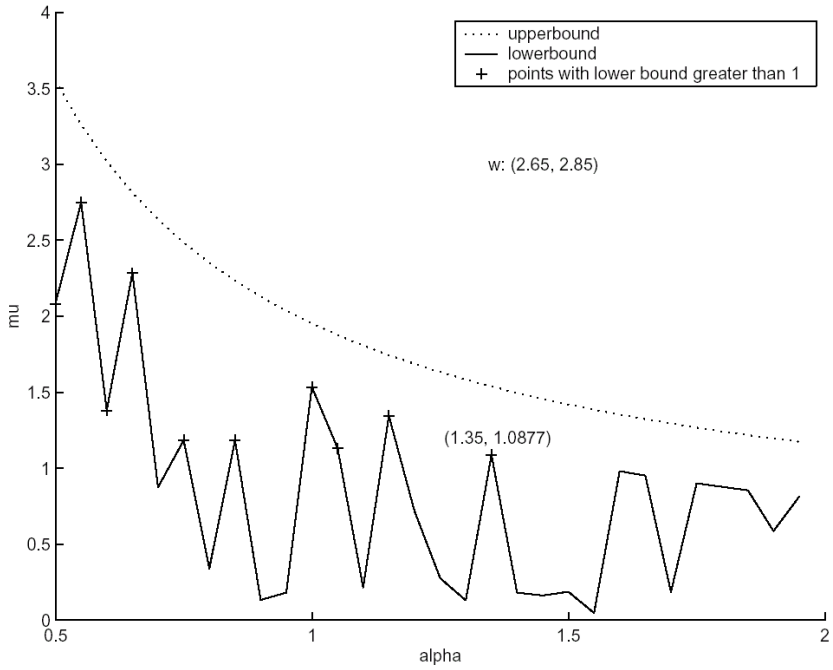

Figure 3.5 α searching to get the skewed-μ

3.4.2 Branch and bound scheme

The test was performed on the four machine system with the same scenario as in the Section 2. The initial frequency range was chosen as [0; 100] r/s. When the tolerance was set to 0.1s, it only took 32.05s to arrive at the results. Large frequency intervals with $\widetilde{\mu} < 1$ were eliminated. The conclusion was that the frequency sweep test should be performed on the intervals [0; 0.19531] r/s and [2.53906; 3.51562] r/s to find the peak value of μ, see Figure 3.6.

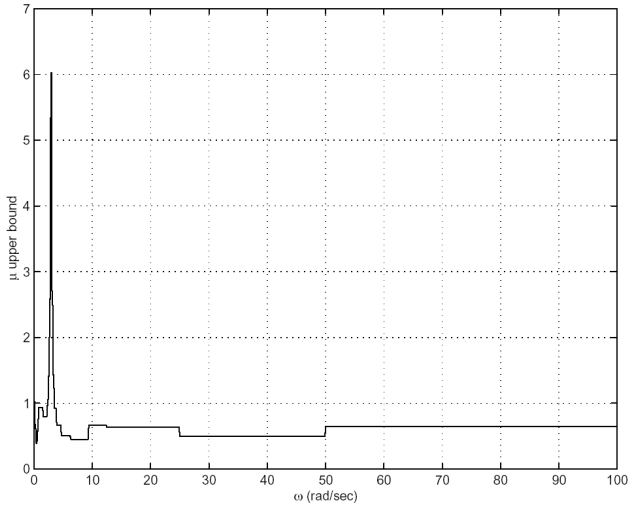

Figure 3.6 μ upper bound from the branch and bound scheme

The frequency sweep followed in this procedure immediately ruled out the former interval and determined the peak of $\mu_{\Delta}(M(j\omega))$. Figure 3.7 is the μ plot for the frequency sweep in the interval [0; 0.19531] r/s, and Figure 3.8 is the μ plot for the frequency sweep in the interval [2.53906; 3.51562] r/s. The peak of μ is 1.4605 at ω = 2.7384. This compares very closely to the value of μ obtained by the exhaustive frequency sweep for the same case in Table 2.1.

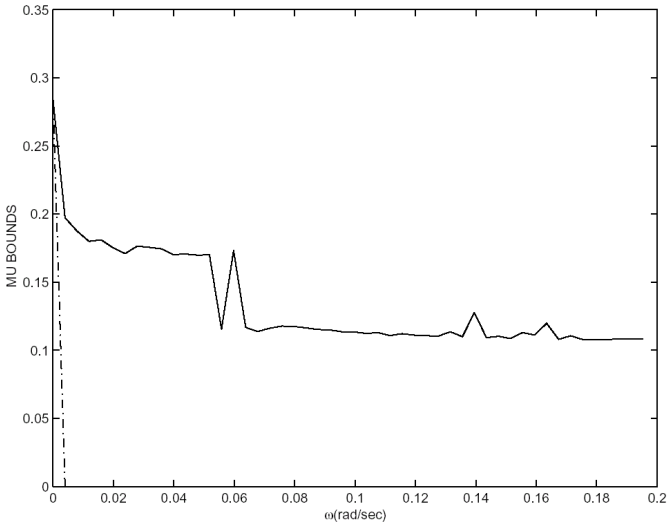

Figure 3.7 Frequency sweep for [0; 0.19531] r/s

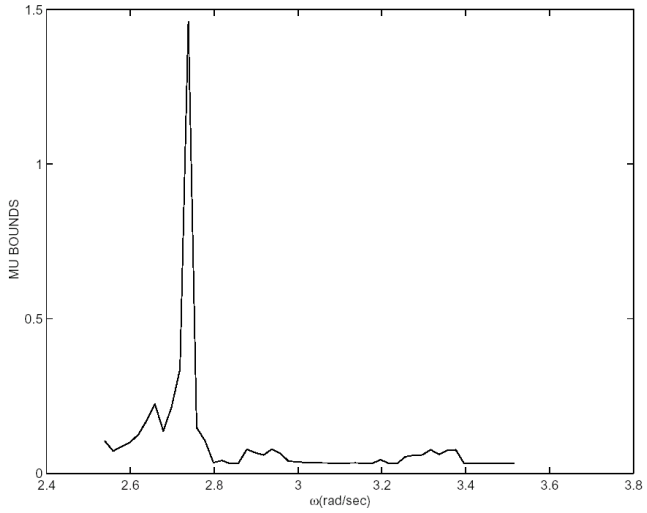

Figure 3.8 Frequency sweep for [2.53906,3.51562] r/s

The proposed branch and bound scheme can efficiently rule out frequency intervals where $\mu_{\bar{\Delta}}(H_1) < 1$ and can narrow the frequency sweep process down to a reasonable frequency interval. This can help us to intelligently select intervals for a frequency sweep and avoid missing important points.

From Figure 3.8, we see that a narrow spike appears in the μ plot. If the frequency sweep test is performed without knowing which frequency interval to pay attention to, it is very easy to miss the peak and, as a result, reach the wrong conclusions. Although the branch and bound scheme takes additional time before performing the frequency sweep, it not only saves time in determining the frequency interval to sweep, but also avoids missing important frequency ranges.

These results demonstrate the advantages of the new branch and bound scheme, and its ability to correctly identify the frequency range in which to perform the frequency sweep to determine the peak value of μ. This will significantly reduce the computational burden for robust analysis of large power systems.

4 Efficient Evaluation of Skewed-μ Bounds

In Section 3.2 the "Skewed-μ" formulation was introduced. In this section, we will build on this formulation and develop efficient techniques to determine the upper and lower bounds for the skewed-μ. Formulation of frequency as an uncertainty parameter is a skewed-μ problem. Previously work with robust analysis of power systems formulated the skewed- μ problem, but calculated μ over a region of frequencies. The resulting answer could only indicate if there was a potential problem in the frequency interval (yes/no) due to the interdependency of frequency in the calculation of μ.

If frequency is skewed (fixed in range) in the problem, the resulting answer is a stability characterization according to the variation of all the other perturbed variables. In short, a stability characterization is obtained for the power system that is guaranteed across precisely the frequency range of operation specified in the perturbation variable.

To explain the concept of skewed- μ more succinctly, consider a value of μ = 1.1 in relation to a robust stability problem. This means that all the perturbations in the system must be decreased in magnitude by a factor of 1.1 to guarantee stability. But what if the desire is to have the uncertainty range of some perturbations fixed, then how large can the other sources of uncertainty be before instability is encountered. This value that quantifies how large the other sources can be is defined as skewed-μ.

In power systems analysis, the skewed variable will be frequency. This implies the question "If frequency is fixed to a certain range, then how large can the other system perturbations be before instability is encountered?" This is precisely the result that is desired. In relation to the system uncertainties, we can quantify the system stability over a specific frequency range and guarantee that there are no missed points. Frequency gridding cannot guarantee unmissed points. Skewed-μ performs a worst-case search over frequency, guaranteeing the answer.

4.1 Skewed-μ mathematical description

The mathematical description of skewed-μ is similar to that of μ and is developed in relation to the standard Linear Fractional Transform (LFT) like Figure 4.1. As an added convenience, the fixed and varying perturbations, and their corresponding sections of *M,* are grouped such that Figure 4.2 holds. In other words, the fixed perturbations are now in the upper left partition and the varying perturbations are in the lower right partition. This can be done via elementary transformations and does not affect the numerical or theoretical results.

Definition 1 *The skewed structured singular value* $\mu_s(M)$ *of a matrix* $M \in \mathbb{C}^{m\times n}$ *with respect to a block structure* $\mathcal{K}_f(m_{r_f}, m_{c_f}, m_{C_f})$ *and* $\mathcal{K}_v(m_{r_v}, m_{c_v}, m_{C_v})$ *is defined as:*

$$\mu_s(M) = \frac{1}{\min\limits_{\Delta \in W_{\mathcal{K}_f,\mathcal{K}_v}} \{\overline{\sigma}(\Delta_v) |\ det(I - \Delta M) = 0 for\ structured\ \Delta\}}$$

with $\mu_s(M) = 0$ *if no* $\Delta \in W_{\mathcal{K}_f,\mathcal{K}_v}$ *solves* $det(I - \Delta M) = 0$.

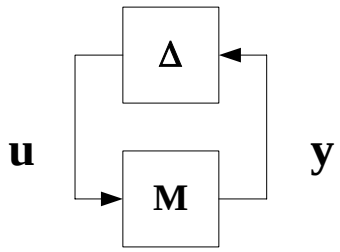

Figure 4.1 Standard LFT form used in robust analysis

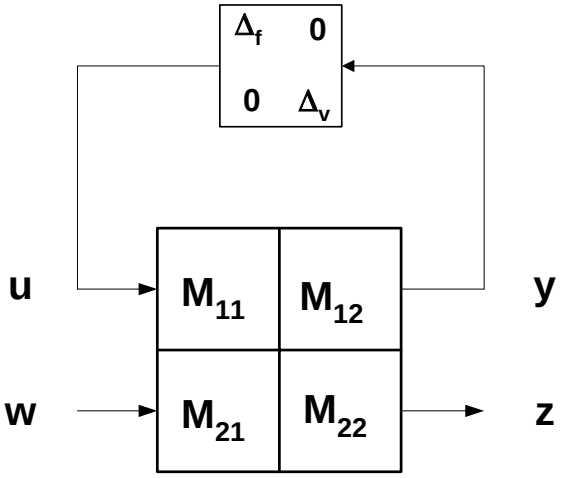

Figure 4.2 LFT form with perturbations arranged into fixed and varying blocks

The block structure of the perturbations can be defined as follows. Given a matrix

$$M \in \mathbb{C}^{m \times n}$$

which interacts with perturbations of a fixed and varying nature, then, define three non-negative integers relating to the number of fixed perturbations m_{r_f}, m_{c_f}, and m_{C_f} with $m_f := m_{r_f} + m_{c_f} + m_{C_f} \leq n_f$, where n_f is the total number of fixed perturbations. The block structure $\boldsymbol{K}_f\left(m_{r_f}, m_{c_f}, m_{C_f}\right)$ is an *m*-tuple of positive integers

$$\mathcal{K}_f = (k_1, \ldots, k_{m_{r_f}}, k_{m_{r_f}+1}, \ldots, k_{m_{r_f}+m_{c_f}}, k_{m_{r_f}+m_{c_f}+1}, \ldots, k_{m_{r_f}+m_{c_f}+m_{C_f}}).$$

Similarly, define for varying perturbations three non-negative integers relating to the number of varying perturbations m_{r_v}, m_{c_v}, and m_{C_v} with $m_v := m_{r_v} + m_{c_v} + m_{C_v} \leq n_v$, where n_v is the total number of varying perturbations. The block structure $\boldsymbol{K}_v\left(m_{r_v}, m_{c_v}, m_{C_v}\right)$ is an *m*-tuple of positive integers

$$\mathcal{K}_v = (k_1, \ldots, k_{m_{r_v}}, k_{m_{r_v}+1}, \ldots, k_{m_{r_v}+m_{c_v}}, k_{m_{r_v}+m_{c_v}+1}, \ldots, k_{m_{r_v}+m_{c_v}+m_{C_f}}).$$

It is also required that

$$\sum_{i=1}^{m} k_{f_i} + \sum_{i=1}^{m} k_{v_i} = n$$

in order that these dimensions are compatible with M.

This determines the set of allowable perturbations, namely define for the fixed perturbations (note that the subscript f is dropped to avoid more clutter):

$$\begin{aligned} Z_{\mathcal{K}_f} = \{\Delta_f = block\ diag(&\delta_1^r I_{k_1}, \ldots, \delta_{m_r}^r I_{k_{m_r}}, \delta_1^c I_{k_{m_r+1}}, \\ &\ldots, \delta_{m_c}^c I_{k_{m_r+m_c}}, \Delta_1^C, \ldots, \Delta_{m_C}^C) : \delta_i^r \in \mathbb{R}, \delta_i^c \in \mathbb{C}, \\ &\Delta_i^C \in \mathbb{C}^{k_{m_r+m_c+i} \times k_{m_r+m_c+i}}\}. \end{aligned}$$

The varying perturbations requires a similar definition (with subscript v dropped):

$$\begin{aligned} Y_{\mathcal{K}_v} = \{\Delta_v = block\ diag(&\delta_1^r I_{k_1}, \ldots, \delta_{m_r}^r I_{k_{m_r}}, \delta_1^c I_{k_{m_r+1}}, \\ &\ldots, \delta_{m_c}^c I_{k_{m_r+m_c}}, \Delta_1^C, \ldots, \Delta_{m_C}^C) : \delta_i^r \in \mathbb{R}, \delta_i^c \in \mathbb{C}, \\ &\Delta_i^C \in \mathbb{C}^{k_{m_r+m_c+i} \times k_{m_r+m_c+i}}\}. \end{aligned}$$

Note that for a matrix M, and a given a set of perturbations, the definition of skewed-μ is the smallest SSV (Structured Singular Value) of a subset of perturbations that destabilizes the system M with the remainder of the perturbations being of fixed size. Formally stating the restriction on perturbations of a fixed size,

$$\mathbf{B}Z_{\mathcal{K}_f} = \{\Delta_f \in Z_{\mathcal{K}} : \overline{\sigma}(\Delta_f) \leq 1\}$$

with the composite Δ perturbations as

$$W_{\mathcal{K}_f, \mathcal{K}_v} = \{\Delta = block\ diag(\Delta_f, \Delta_v)\}.$$

Here **B** represents then n_f dimensional ball of Δ_f, which is restricted to a perturbation of size 1. The unit ball is indicated as a formality. In practice, the fixed perturbation has some fixed range, -1 to 10, 0 to 100, -50 to 50, etc., to which it is restricted. These ranges are normalized to unity and the associated scalings absorbed into M.

The difficulty in this definition of skewed-μ is that skewed-μ is believed to be NP hard; i.e., it cannot be calculated in polynomial time. The means of approaching a calculation for skewed-μ is through the implementation of bounds. This is similar to the case of the standard μ problem. Hence, there is a natural point to begin from when progressing towards skewed-μ bounds.

The development of these bounds is one of the primary steps in assessing the stability of the power systems. Upper and lower bounds for skewed-μ are developed, both theoretically and computationally.

4.2 Skewed-μ lower bound

The skewed-μ lower bound was developed first and has been published in the American Controls Conference Proceedings 2002 [17]. The premise for the lower bound is to find a unitary matrix Q that maximizes the real spectral radius (ρ_R) of a matrix M. This skewed-μ lower bound can be expressed as

$$\mu_s(M) \geq \rho_R(QM),$$

where the spectral radius has been found using the eigenvalue equation:

$$QMx = Sx.$$

This is the eigenvalue equation with a requirement that S be arranged as a partitioned matrix

$$S = \left[\begin{array}{c|c} I_f & 0 \\ \hline 0 & \nu I_v \end{array}\right].$$

instead of the standard configuration of

$$QMx = \lambda x.$$

In the matrix S, ν represents the eigenvalue to be solved for. The reason for constructing the partitioned, scaled matrix S is to keep the solution to part of the system of equations fixed (skewed) while varying the solution to the remainder of the system of equations via ν so that the largest spectral radius may be found. This explanation also assumes the matrix M has been rearranged via elementary transformations to allow the rows of M interacting with fixed perturbations to occupy the first n_f positions, with the remaining n_v rows being occupied by the rows that interact with the varying perturbations, as described earlier. This is a convenience only, and aids the theoretical development as well as the computational algorithmic development.

To maximize ρ_R, a gradient search using the derivative of an eigenvalue and a power iteration is used to align the right and left eigenvectors while finding Q. When the eigenvectors are aligned, then a Q has been found that achieves a maximum ρ_R. Unfortunately, the lower bound is not convex, hence it is not know if the maximum is local or global; however, the algorithm works well in practice.

4.3 Skewed-μ upper bound

The skewed-μ upper bound was developed second, and has been computationally implemented in two ways. The first way is direct calculation that seeks to find the upper bound on skewed-μ using the concept that skewed-μ is less than the maximum singular value of the portion of M that interacts with the varying range perturbations. Using S to scale the portion of M that interacts with the varying range perturbations, the upper bound of skewed-μ can be found from

$$\overline{\sigma}(\sqrt{S^{-1}}DMD^{-1}\sqrt{S^{-1}}) \leq 1$$

where S is as previously defined. This gives an upper bound on skewed-μ as

$$\mu_s \leq \nu$$

In the two previous equations, $\overline{\sigma}$ represents the maximum singular value, D represents a matrix norm balance via Osborne methods [18], and S represents a scaling matrix used for scaling the sections of M which interact with the varying perturbations. These matrices can be expanded as

$$\overline{\sigma}\left(\begin{bmatrix} I_f & 0 \\ 0 & \frac{1}{\sqrt{\nu}} \cdot I_v \end{bmatrix} \begin{bmatrix} d_1 & & \\ & \ddots & \\ & & d_n \end{bmatrix} \begin{bmatrix} M_{11} & M_{12} \\ M_{21} & M_{22} \end{bmatrix} \begin{bmatrix} d_1^{-1} & & \\ & \ddots & \\ & & d_n^{-1} \end{bmatrix} \begin{bmatrix} I_f & 0 \\ 0 & \frac{1}{\sqrt{\nu}} \cdot I_v \end{bmatrix}\right) \leq 1$$

To make coding the computational algorithm more convenient, the system has been normalized, and arranged via elementary transformations such that the fixed range perturbations occupy the upper left quadrant of the perturbation matrix, and the varying range components occupy the lower right quadrant of the perturbation matrix as previously discussed. Since the singular values of a matrix P are the eigenvalues of the matrix $P^H P$, the resulting matrix of

$$P = \sqrt{S^{-1}} D M D^{-1} \sqrt{S^{-1}}$$

was manipulated into the generalized eigenvalue problem form,

$$Ax = \lambda Bx$$

where the value of ν could be calculated directly using standard Matlab® tools. The resulting value ν is an upper bound on skewed-μ.

The second procedure for finding an upper bound on skewed-μ was developed by deriving an expression for the skewed-μ upper bound as an LMI (Linear Matrix Inequality),

$$\mu_s(M) \leq \inf_{D \in \mathcal{D}} \min_{0 \leq \nu \in \mathbb{R}} \left\{ \nu : M^H D^H D M - \begin{bmatrix} I_f & 0 \\ 0 & \nu^2 \cdot I_v \end{bmatrix} D^H D \leq 0 \right\},$$

where M is the matrix describing the nominal system, D is the norm balancing matrix, and the partitioned identity matrix with scaling factor ν represents the setup for solving for the smallest singular value to the system M where the partition has been implemented to force the solution of this equation over the portion of the system that with varying perturbations (I_v). This is a variation to the standard form of the Generalized Eigenvalue Problem (GEVP) [19], and was developed for finding the skewed- μ upper bound.

Some of the computational aspects for the LMI upper bound led to the use of the Matlab® LMI toolbox for implementation of the LMI upper bound calculation. This provides excellent results for smaller problems, but becomes overburdened on the large power system problems. This area is seen as a place for improvement, since the general purpose LMI toolbox appears significantly slower than the special purpose LMI solver used for calculating an upper bound on μ in the μ tools toolbox.

The results obtained from the skewed-μ upper bound research have resulted in two theoretical bounds, and two computational algorithms programmed in Matlab®.

4.4 Results of skewed-μ software tools testing

When the skewed-μ computational tools were applied to the 4-machine test system, the results provided a bound that was not as close to the projected results as other tools listed in this document. The primary reason for this involves the Matlab® LMI toolbox. The number of parameters in the 4-machine problem overwhelms the capabilities of the LMI toolbox; hence the second, more accurate upper bound method could not be applied. Only the first upper bound method could be used. Calculations involving the original μ code do not have this problem because they use a specifically designed system for finding the μ upper bound, including a gradient descent algorithm coupled with a modified LMI solver. Inspecting the underlying μ code shows that the values calculated by the μ tool and skewed-μ tool have similar values with respect to the 4-machine test system. It is only in the later stages of the μ tool upper bound software that significant improvements are made in the computation of the μ upper bound. This result indicates that an extension of the gradient descent algorithm coupled with a modified LMI solver from the original μ software to a similar method for the skewed-μ software tools is needed. This extension would include some theoretical development as well as creation of software tools.

Figure 4.3 shows the results for the skewed-μ upper bound of the 4-machine test system over the most significant frequency range. This figure was obtained by applying the first method for finding the skewed-μ upper bound. The second skewed-μ upper bound method using an LMI could not be implemented due to problem size restrictions.

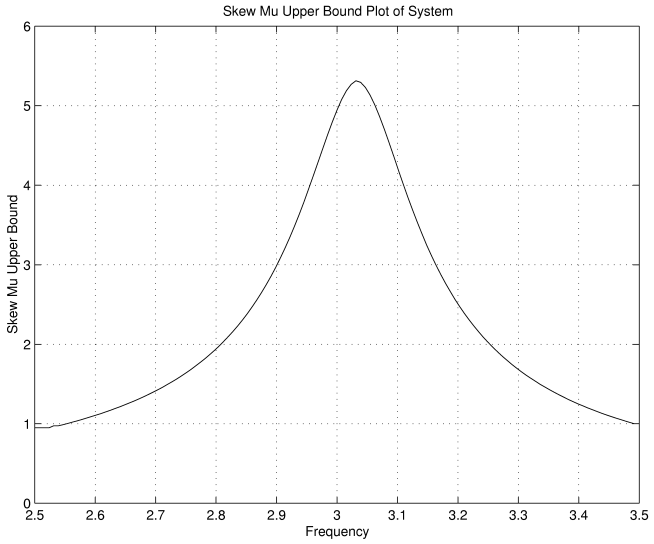

Figure 4.3 Skewed- μ upper bound for 4-machine system-frequency detail

It should be noted that on smaller test problems with systems placed in a skewed-μ format, the skewed-μ tool performed well. In these cases the skewed-μ tool used its LMI capabilities as well as the first method for finding the skewed-μ upper bound.

Figure 4.4 shows the results for the skewed-μ upper bound of the 4-machine test system over the full frequency test range and is similar to the results obtained from the branch and bound scheme for the same frequency range shown in Figure 3.6.

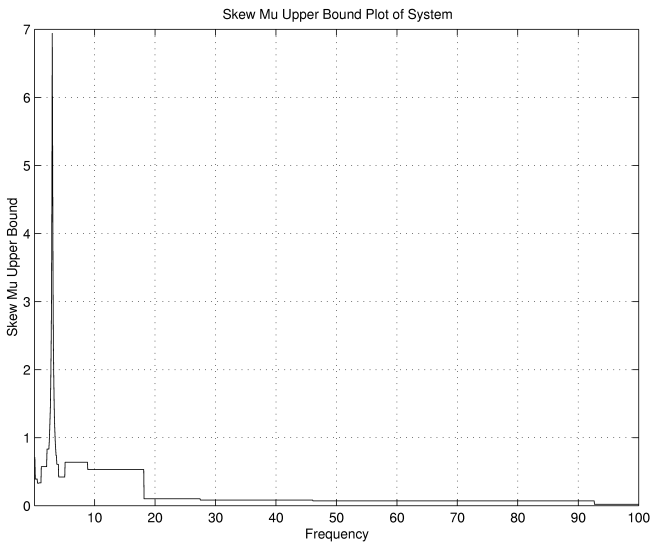

Figure 4.4 Skewed-μ upper bound for 4 machine system-full frequency span

The results of the skewed-μ upper and lower bound testing indicate that the developed methods hold considerable promise. However, other associated algorithms used in the determination of these bounds need to be improved. This should be considered as a future research issue that will be addressed.

5 Control Design Using H_∞ Loop Shaping

In the previous sections we have dealt with techniques to improve the computational aspects of the SSV or μ-tools for robust stability analysis. We have made some important strides in improving the computational aspects of the μ-bounds. Our work also showed that further work is needed in improving some computational tools that are necessary to determine the μ-bounds. With this development in mind, we now look at an alternate approach that can result in significant savings in computational time for the design of controls in large power systems. H_∞ with loop shaping is an alternative approach to design controls for large power systems. This approach introduced by McFarlane and Glover [20] is an elegant design process that has several advantages [15].

- It is easy to apply and works very well in practice.
- The solution procedure is non-iterative, and explicit formulas for the corresponding controllers are available.
- For a selected nominal plant, there is a closed formula for the maximum stability margin.
- Except for special systems (that is, systems with all-pass factors), there are no pole-zero cancellations between the plant and controller. Pole-zeros cancellations are common in many H_∞ control problems and are a problem when the plant has lightly damped modes.

Ever since this design procedure was proposed, there have been many applications in industry. For power systems, Ambos [22], Pannett [23] et al used the procedure to design a controller for generator control. Graham [24] has designed robust controllers for FACTS devices to damp low frequency oscillations. In light of these successful applications, we introduce this design procedure to PSS design, and provide some basic guidelines for loop shaping weighting selection and controller design paradigm formulation.

5.1 H_∞ loop shaping design

The Glover-McFarlane H_∞ loop shaping design procedure consists of three steps.

1. Loop Shaping. In loop shaping design, the closed-loop performance is specified in terms of requirements on the open-loop singular values. The open loop singular values are then shaped to give desired high or low gain at frequencies of interest. This step takes advantage of the conventional loop shaping technique, but no phase requirements need to be considered. That is, the closed-loop stability requirements are disregarded since the H_∞ synthesis step taken thereafter will robustly stabilize the shaped plant. Using a precompensator W_1 and/or a postcompensator W_2, the singular values of the nominal plant are shaped to give the desired open-loop shape. The nominal plant G, the shaping functions W_1 and W_2 are combined to form the shaped plant, G_s where $G_s = W_2 G W_1$. We assume that W_1 and W_2 are such that G_s contains no hidden modes.

2. Robust Stabilization. It has been shown that the largest achievable stability margin $\varepsilon_{\max}$ can be obtained by a non-iterative method [20]. $\varepsilon_{\max}$ is the stability margin for the normalized coprime factor robust stability problem(see section III-A in [20]). It provides a robust stability guarantee for the closed loop system. Suppose $\widetilde{M}_s$, $\widetilde{N}_s$ are normalized left coprime factors of G_s such that $G_s = \widetilde{M}_s^{-1}\widetilde{N}_s$, then

$$\varepsilon_{\max} = \left(1 - \left\|\left[\widetilde{M}_s, \widetilde{N}_s\right]\right\|_H^2\right)^{1/2} \tag{5.1}$$

where $\| \ \|_H$ denotes the Hankel norm. The controller is now defined by selecting $\varepsilon \le \varepsilon_{\max}$, and then synthesizing a stabilizing controller K_∞, which satisfies

$$\left\| \begin{bmatrix} I \\ K_\infty \end{bmatrix} \left(I - G_s K_\infty\right)^{-1} \widetilde{M}_s^{-1} \right\|_\infty \le \varepsilon^{-1}$$

3. The final feedback controller is given by $K = W_1 K_\infty W_2$. It has been proven [20] that the degradation of the open-loop shape due to the inclusion of K_∞ is limited.

Figure 5.1 provides a schematic overview of the procedure.

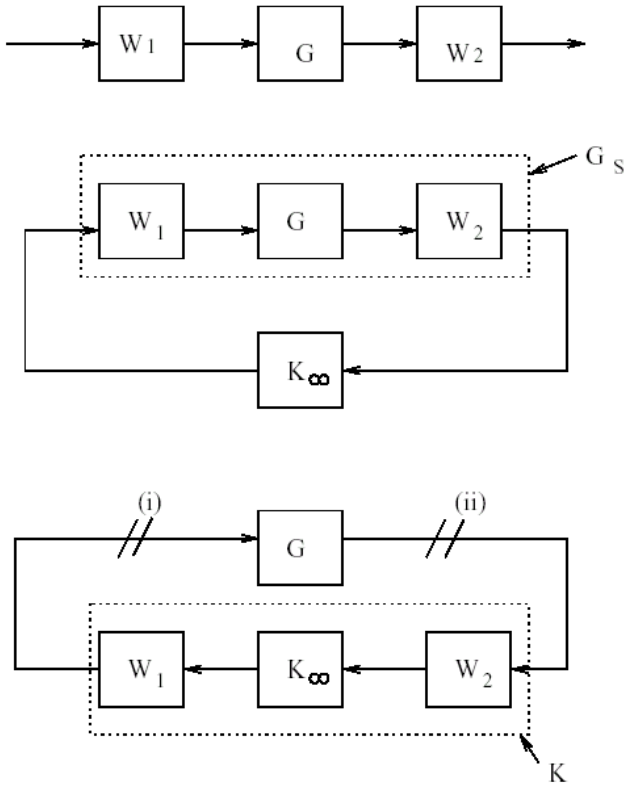

Figure 5.1 The loop shaping design procedure

5.2 Power system models

To study the control of power system oscillations, the two-area, four-machine system described in Section 2.7 was used. In this system, the synchronous machines are modeled with the two-axis model [24]. The generators are equipped with the IEEE AC-4 excitation system [24] (see Figure 2.1). It has been shown by Kundur [25] that the case when only one conventional PSS is installed at the machine close to the tie line in the sending area has the worst performance and stability behavior. It even destabilizes the most stressed plant. We choose this case to design our controller. The 50-Generator IEEE Test system described in Section 2.7 is also used for testing the design approach.

The linearized system models, including the generators, exciters, and the networks, have the following state space representation:

$$\begin{aligned} \dot{x} &= \widetilde{A}x + \widetilde{B}u + \widetilde{B}d \\ y &= \widetilde{C}x + \widetilde{D}u \end{aligned} \tag{5.2}$$

where x is a vector of the state variables, u is the control input, d is the disturbance, and y is the output variable. They are defined as follows:

$$\begin{aligned} x^T &= \left[x_{SM}^T, x_{ES}^T\right] \\ x_{SM}^T &= \left[\Delta E'_{q(1-n)}, \Delta E'_{d(1-n)}, \Delta\omega_{(1-n)}, \Delta\delta_{(2-n)1}\right] \\ x_{ES}^T &= \left[\Delta E_{FD(1-n)}, \Delta X_{E1(1-n)}, \Delta X_{E2(1-n)}\right] \\ u &= \left[\Delta V_{PSS}\right] \\ d &= \left[\Delta V_{REF}\right] \\ y &= \left[\omega_\Delta\right] \end{aligned}$$

where ω_Δ is the relative rotor speed, and $\omega_\Delta = \dfrac{\omega_i}{\omega_s} - 1$. $\widetilde{A}, \widetilde{B}, \widetilde{C}$, and $\widetilde{D}$ are coefficient matrices which depend on the operating conditions.

5.3 Controller design for the four-machine system

The specific feedback structure for our problem is formed and the H_∞ loop shaping design procedure is applied as shown in Figure 5.2. The first step is to choose the weighting function W_a to shape the open-loop system so as to make the closed-loop system achieve good disturbance attenuation. The shaping objective is to make the output $y = \omega_\Delta$ (the generator speed variation) as small as possible with disturbance signal $d = \Delta V_{REF}$. Since the frequency of the inter-area mode is around 3 rad/sec, the performance objective has been translated to increase the open-loop gain around that frequency.

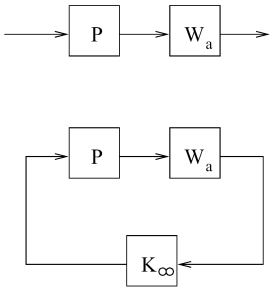

5 2. The H_∞ loop shaping design

After that, an H_∞ controller, K_∞, was synthesized to ensure the robust stability of the closed-loop system. Finally, K_∞ was cascaded with the shaping function W_a to form the final controller $K = K_\infty W_a$. Figure 2.5 shows the four-machine, two-area test system. The exporting power Pexp from Area 1 to Area 2 through the tie line was chosen as the uncertainty and was allowed to vary in the range [0 - 400] MW by varying the loads and generations in each area. All the four generators are equipped with IEEE AC-4 excitation system. We chose a plant set consisting of five plants that have different exporting power, as shown in Table 5.1. The five plants are all stable but have poorly damped inter-area modes. As stated before, we choose a configuration with the PSS located at the generator at bus 2 to stabilize the system.

Table 5.1 The Perturbed Plant Sets

	P_1	P_2	P_3	P_4	P_5
P_{exp} (MW)	0	100	200	300	400

The five plants are all stable but have poorly damped inter-area modes.

5.3.1 Controller design

1) Loop shaping

P_4 is chosen as the nominal plant. The eigenvalues, damping ratios and the frequencies of the modes for the nominal plant are listed as in Table 5.2.

The eigenvalues -0.0663± j 2.6938 correspond to the inter-area mode. The damping ratio for this mode is only 0.0246. The objective of loop shaping is to increase the open-loop gain around this frequency. To choose the weighting function W_a, we add pole and zero pairs to achieve gain increase in the desired frequency range while keeping the gain change as small as possible around other frequency values. The following transfer function for the weighting was used.

$$W_a = \frac{186.5 \times 10s(1+0.33s)}{(1+10s)(1+0.1852s)}$$

The addition of the zero at the origin forces the controller to have a zero dc gain, thus, ensuring it only works in the transient state. A washout filter block in W_a, with time constant 10s is used to ensure the controller only works in the transient state. The selection of the pole at $\frac{1}{0.1852}$ and the zero at $\frac{1}{0.33}$ increased the gain around the frequency of interest so that the plant input disturbance can be attenuated effectively.

The resulting open-loop gain from the reference voltage variation to the generator speed variation is shown in Fig 5.3.

Table 5.2 The Modes of the Nominal Plant

Eigenvalues	Damping Ratio	Frequency (Hz)
-0.3846		
-0.3405 ± j 0.5160	0.5507	0.0821
-0.3483 ± j 0.5401	0.5419	0.0860
-1.4034		
-1.3996± j 1.0147	0.8096	0.1615
-0.0663± j 2.6938	0.8219	0.2592
-3.6072		
-1.1499±j 7.8488	0.1450	1.2492
-1.0524±j 7.9022	0.1320	1.2577
-9.6413		
-9.7180		
-85.2897		
-86.1091		
-92.5616		
-106.8436		
-106.9204		
-112.2049		
-112.8359		

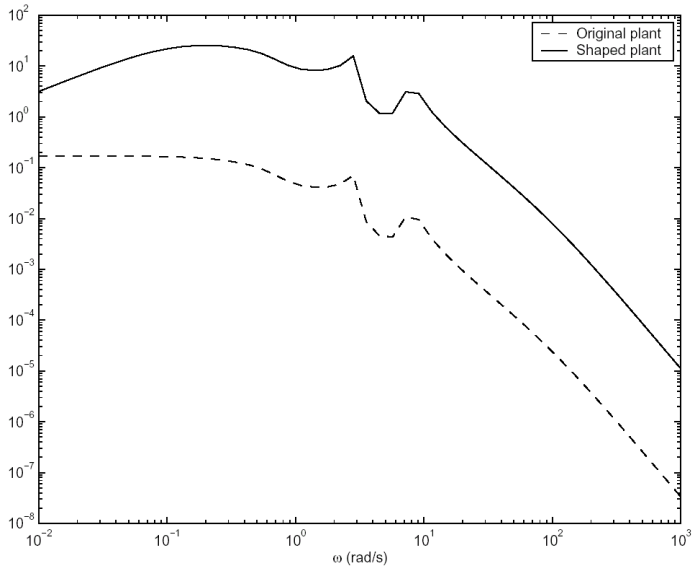

Fig. 5.3. Comparison of the open-loop gains between the original plant and the shaped plant.

2) H_∞ synthesis

Next, we synthesized a K_∞ controller to achieve robust stability for the nominal plant. According to Equation (5.1), the maximum stability margin $\varepsilon_{\max}$ is 0.4975, which is large enough and indicates the feasibility of our loop shaping design. The objective for the H_∞ robust stabilization is:

$$\left\| \begin{bmatrix} I \\ K_\infty \end{bmatrix} \left(I - P_s K_\infty\right)^{-1} \widetilde{M}_s^{-1} \right\|_\infty \le 0.4975^{-1}$$

According to McFarlane and Glover [25], given the normalized left coprime factorization of the nominal plant as $P_{s0} = \widetilde{M}^{-1}\widetilde{N}$, the controller K_∞ can stabilize all $P_s = \left(\widetilde{M}_s + \Delta_M\right)^{-1}\left(\widetilde{N}_s + \Delta_N\right)$ satisfying $\left\| [\Delta_M, \Delta_N] \right\| < 0.4975$. Furthermore, according to Georgiou [27], a controller stabilizes a gap ball of uncertainty with a given radius if and only if it stabilizes a normalized coprime factor perturbation ball of the same radius. Thus, in terms of the gap metric, all P_s with $\delta_g\left(P_s, P_{s0}\right) < 0.4975$ can be stabilized by this controller.

We list the gap between the weighted plants ($P_{si} = P_i W_a$, i = 1,…,5) in Table 5.3. Thus all the plants can be stabilized by this controller, or the controller achieves robust stability.

Table 5.3 The Gap Between the Weighted Plants

$\delta_g\left(P_{s4}, P_{s1}\right)$	$\delta_g\left(P_{s4}, P_{s2}\right)$	$\delta_g\left(P_{s4}, P_{s3}\right)$	$\delta_g\left(P_{s4}, P_{s5}\right)$
0.3463	0.2615	0.1698	0.2215

Here the uncertainties are of the nomalized coprime factorization type. These characterization are more conservative than the parametric uncertainties in the μ approach. The final controller is the combination of W_a with K_∞, that is $W_a K_\infty$. To check the performance of this controller, the frequency response of the closed-loop singular values are given in Fig 5.4. The frequency response of the singular value for all five closed-loop transfer functions (from the voltage disturbance to the generator speed variation) are shown. In Fig 5.4, the gains around the frequency of the inter-area mode (about 3 rad/sec) are small which shows good disturbance attenuation for oscillations with such frequency.

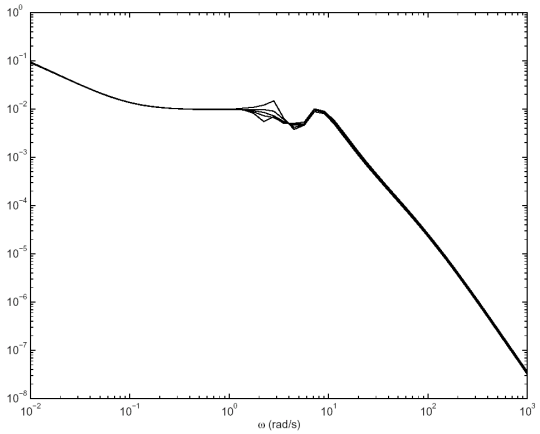

Fig. 5.4. Singular values of closed-loop transfer functions: $\bar{\sigma}\left(\left(I - PK\right)^{-1} P\right)$ **for five plants.**

Table 5.4 shows the damping ratios of the controlled closed-loop systems. The minimum damping ratio for the nominal plant is only 0.0246. After adding the designed controller, the nominal closed-loop systems have a minimum damping ratio of 0.1449. The inter-area mode is well damped. For other perturbed plants, the minimum damping ratio is 0.1245.

Table 5.4 The Modes of the Controlled Nominal Plant

Eigenvalues	Damping Ratio	Frequency (Hz)
-0.0009		
-0.0031		
-0.3271±j 0.4931	0.5528	0.0785
-0.3273 ± j 0.4931	0.5530	0.0785
-0.4186±j 0.6707	0.5295	0.0843
-0.4245±j 0.6687	0.5359	0.0853
-0.9989		
-1.0044		
-0.7646±j 0.9457	0.6287	0.1505
-0.7566±j 0.9652	0.6169	0.1536
-0.5274±j 2.9422	0.1764	0.4683
-0.4686±j 3.0242	0.1531	0.4813
-4.1888±j 0.5136	0.9926	0.0817
-4.2507		
-1.9460±j 4.8502	0.3724	0.7719
-1.2415±j 5.9065	0.2057	0.9400
-6.0387		
-1.1498±j 7.8503	0.1449	1.2494
-1.1498±j 7.8504	0.1449	1.2494
-8.0094±j 0.7452	0.9957	0.1186
-3.6487±j 7.7779	0.4247	1.2379
-9.6396		
-9.8272		
-83.8960±j 1.4739	0.9998	0.2346
-87.5881±j3.8722	0.9990	0.6163
-94.1128±j 5.2698	0.9984	0.8387
-103.7650±j 5.8112	0.9984	0.9249
-110.7216±j 5.1594	0.9989	0.8211
-114.8270±j 2.0315	0.9998	0.3233

We would also like to see how much the open-loop shape has been changed because of the inclusion of K_∞. Comparing the curves in Fig 5.5, it can be seen that the robust stabilization stage has not significantly altered the desired loop shape.

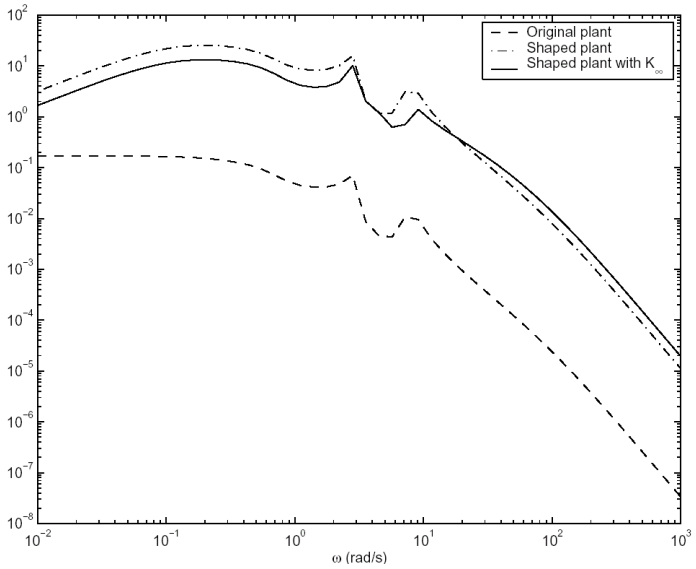

Figure 5.5 Comparison of open loop singular values

3) Controller order reduction

We want to conduct a nonlinear simulation using ETMSP [24] to examine the performance of the designed controller. The resulting controller has a high order (27th) while ETMSP can only handle a user defined model up to the 8th order. The controller is reduced to a 7th order controller using the Hankel Norm reduction.

The transfer function of the reduced order controller is given as $G_k(s) = \frac{N(s)}{D(S)}$, with

$$N(s) = 583.3s^7 + 10828s^6 + 82531s^5 + 588160s^4 + 2.49\times10^6 s^3 + 4.97\times10^6 s^2 + 1.03\times10^7 s - 36500$$

$$D(s) = s^7 + 41.3s^6 + 549.6s^5 + 2895.8s^4 + 18506s^3 + 34149s^2 + 1.1\times10^5 s + 9516.6$$

The bode plots of the full-order controller and the reduced-order controller are shown in Fig 5.6.

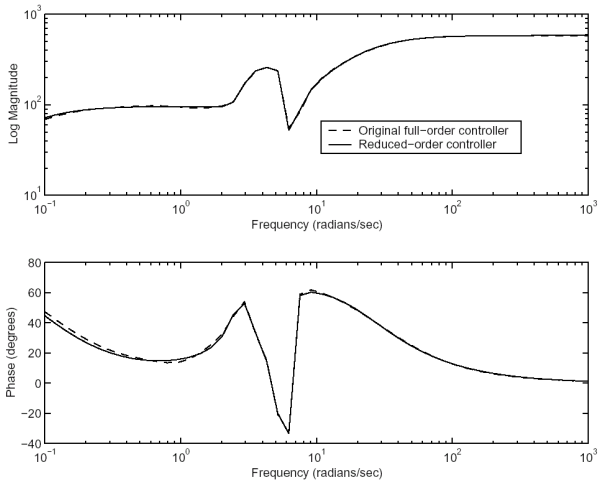

Figure 5.6 Bode plots comparison of full-order controller and the reduced-order controller

5.3.2 Simulation results on the four-machine system

1) Nonlinear Simulations

Nonlinear simulations are performed using ETMSP to test the efficacy of the designed controller. Three-phase short circuits are applied and cleared for a certain duration; the tie line real power flow is monitored. The performance of the designed controller is compared with that of a conventional PSS, which has been tuned using the procedure described in [27]. Its block diagram is shown as in Figure 2.2. The comparison is also made between the H_∞ loop shaping controller and a μ controller obtained from the DK-iteration [11] procedure. Its transfer function is given as $G_\mu(s) = \dfrac{N_\mu(s)}{D_\mu(s)}$, with

$$N_\mu(s) = -0.00013s^8 + 1.139\times10^5 s^7 + 8.655\times10^5 s^6 + 9.382\times10^6 s^5 + 4.367\times10^7 s^4 + 9.919\times10^7 s^3 + 1.749\times10^8 s^2 + 9.868\times10^7 s + 3.247\times10^7$$

$$D_\mu(s) = s^8 + 148s^7 + 3850s^6 + 1.604\times10^4 s^5 + 1.739\times10^5 s^4 + 4.546\times10^5 s^3 + 1.367\times10^6 s^2 + 1.357\times10^6 s + 6.589\times10^5$$

Figure 5.7 shows it's bode plot.

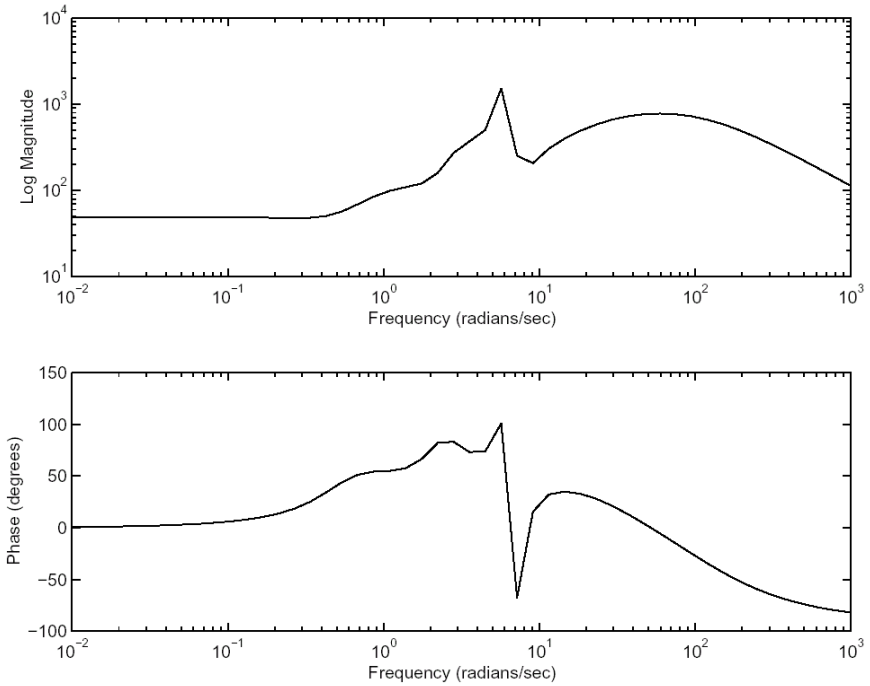

Figure 5.7 Bode plot for the μ controller

2) Fault at bus 6 cleared after 10ms.

The conventional PSS is designed for the case where the tie line exporting power is 0MW. It works well and has a good damping effect under this specific operating condition (see Figure 5.8). But when the operating point changes and the system becomes more stressed, the improperly tuned PSS even destabilizes the system (see Figure 5.9). It is observed that the PSS designed using the loop shaping procedure and the H_∞ approach provides good damping in the entire range of operating conditions.

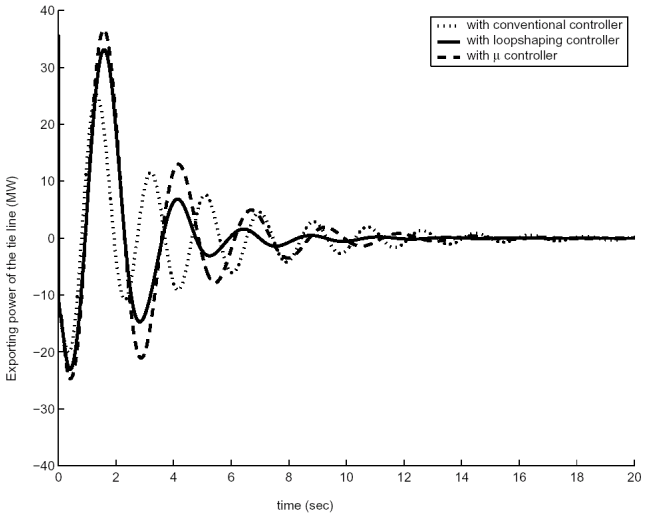

Fig. 5.8. Comparison among the H_∞ loop shaping controller, μ controller and the conventional controller (3 phase fault at bus 6 and 0MW exporting power case).

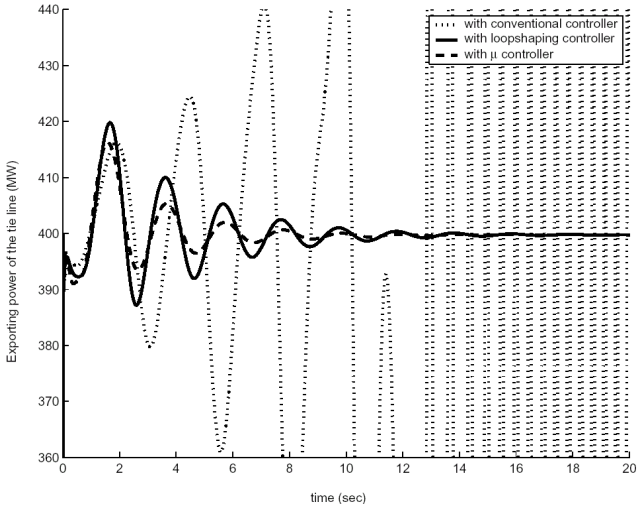

Fig. 5.9. Comparison among the H_∞ loop shaping controller, μ controller and the conventional controller (3 phase fault at bus 6 and 400MW exporting power case).

From the simulation results shown in Figure 5.8 and Figure 5.9, we see that both the μ controller and H_∞ loop shaping controller achieve robust performance and damp the oscillations very well for the whole operating range. The μ controller provides slightly better damping. However, the design procedure for the μ controller is more complex than the H_∞ loop shaping. Besides the selection of the weighting function, it involves DK-iterations and will generate a controller with a much larger order than the H_∞ loop shaping controller.

3) Fault at bus 5 cleared after 10ms.

Similar comparisons are made for this fault. This is a fault in the area exporting energy. The conventional PSS does not work well for this case, see Figure 5.10 and Figure 5.12.

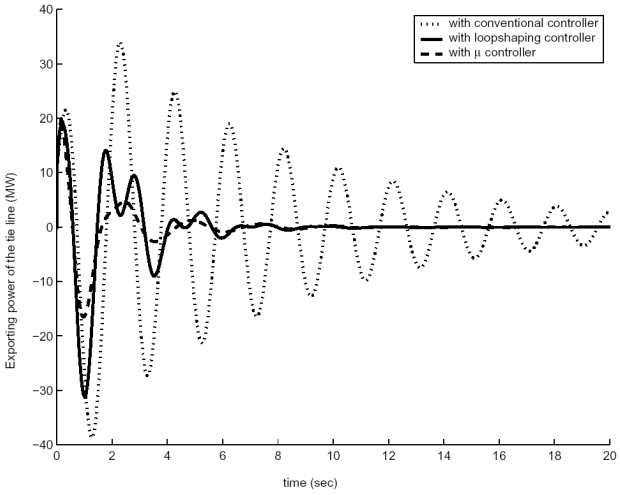

5.10 Comparison among the H_∞ loop shaping controller, μ controller and the conventional controller (3 phase fault at bus 5 and 0MW exporting power case)

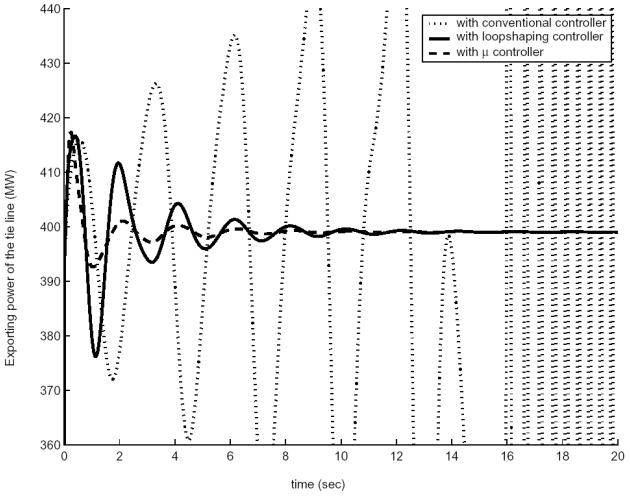

Fig. 5.11. Comparison among the H_∞ loop shaping controller, μ controller and the conventional controller (3 phase fault at bus 5 and 400MW exporting power case).

Comparisons are also made between the performance of μ controller and that of the H_∞ loop shaping controller, as shown in Figure 5.10 for 0MW exporting power case and in Figure 5.11 for the 400MW exporting power case. These conditions represent the limiting cases for the range of operation considered. Both controllers have good damping ability. The μ controller provides slightly better damping than the loop shaping controller.

5.3.3 Robustness validation

The structured singular value (SSV) based robust analysis is performed to validate the robustness of the resulting controller [28]. The process of characterizing the uncertainties and the definition of SSV are summarized in Section 2.

The value of peak μ over the frequency reflects the robustness of the controller. Its inverse is the maximum parameter which can still let the system maintain stability. For the normalized uncertainty, a value of peak μ which is greater than 1 indicates that the controller cannot achieve robust stability. The μ analysis results for the three controllers are listed as in Table 5.5. From the table we see that both the H_∞ loop shaping controller and the μ controller can achieve robust stability while the conventional PSS is not robust. The μ controller is more robust than the H_∞ loop shaping controller.

Table 5.5 The peak μ values for the three types of controllers

Controller	Peak μ value
H_∞ loop shaping controller	0.62
μ controller	0.42
conventional PSS	3.0

5.4 Controller design for a fifty-machine system

The loop shaping design was also applied to a fifty-machine system. This is a moderate-sized system which includes all the modeling features and the complexity of large scale power systems. A one-line diagram of the area of interest is shown in Figure 2.6. This test system contains 44 generators represented by the classical model with uniform damping and 6 generators represented by a two-axis model. The base case power flow was characterized by setting the generation at Bus #93 and #110 to be 1250MW. This generation varies in the range [2 × 1150 - 2 × 1350] MW. Four sequentially designed PSSs using Glover-McFarlane loop shaping approach are located on generators #93, #104, #110 and #111. The weighting function for each loop was chosen as

$$W_a = \frac{1865s}{1+10s}$$

The high gain of 1865 is applied to improve the open loop gain for all frequencies. The additional zero at the origin which forces the system to have a zero dc gain and the washout filter with time constant 10s ensure the controller only works in the transient state. Comparisons of the open-loop gains between the original plant and the shaped plant after installing the four PSSs sequentially are shown as in Figure 5.12.

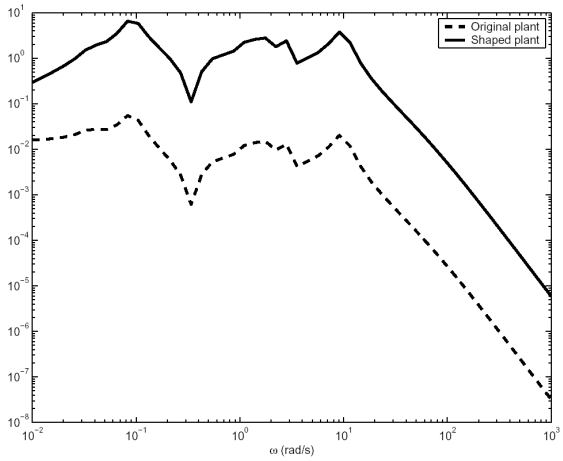

Fig. 5.12. Comparison of the open-loop gains between the original plant and the shaped plant (Original plant has 3 loop shaped PSSs) for the PSS at generator #111).

Nonlinear simulations are performed using ETMSP. A three-phase short circuit is applied at Bus #33 and cleared after 10ms. The active power of generation #110 is monitored. The performance of the designed controllers is compared with that of a conventional controller, see Figures 5.13 and Figure 5.14.

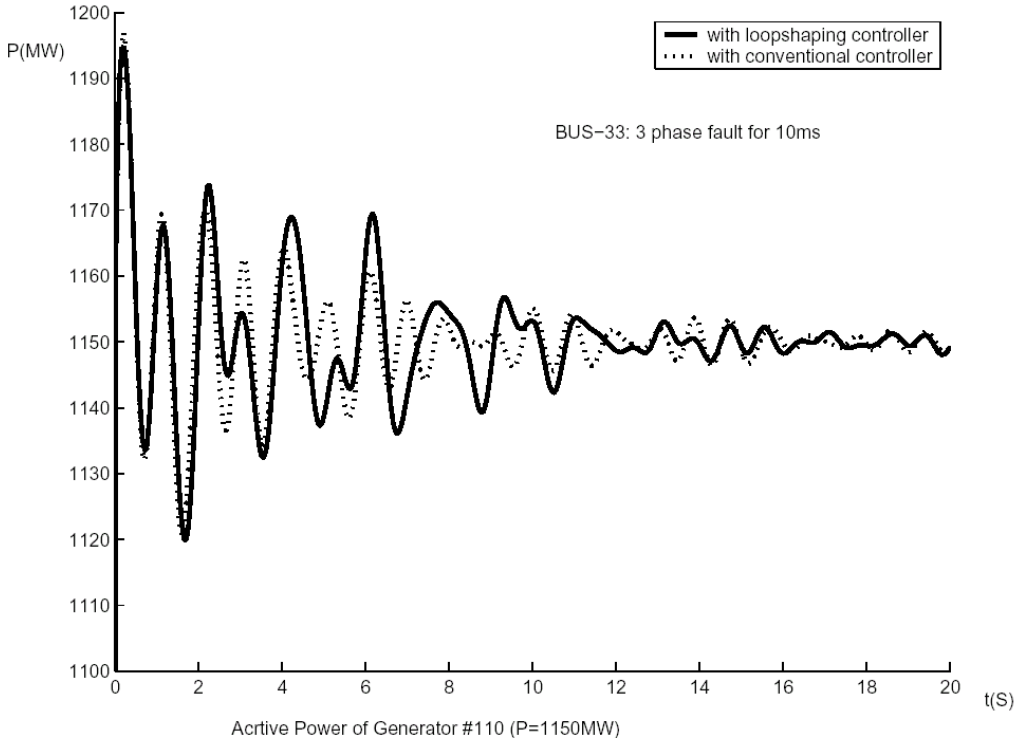

Fig. 5.13 Comparison of the performance between the H_∞ loop shaping controller and the conventional PSS at 1150MW

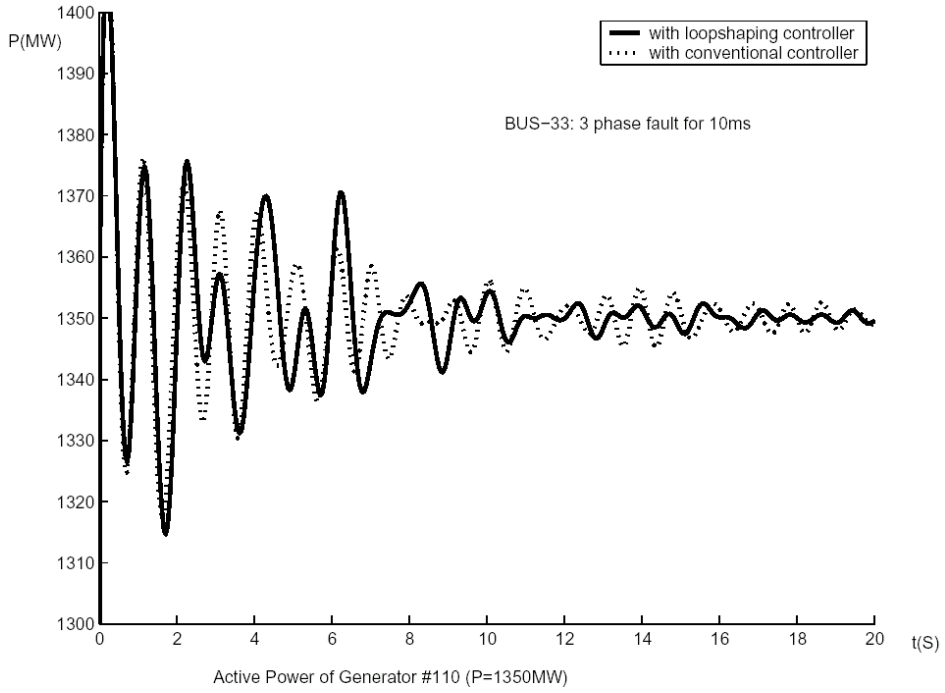

Fig. 5.14 Comparison of the performance between the H_∞ loop shaping controller and the conventional PSS at 1350MW.

It can be seen from the figures that the H_∞ loop shaping controller demonstrates better robustness than the conventional PSS.

Another case was prepared to show the better performance of the H_∞ loop shaping controller over the conventionally designed PSS in the range of operation considered. Both generator #93 and generator #110 output real power were set at 1580MW. A three phase fault is applied to bus #7 for 10 ms, the fault is cleared by opening the line between bus #7 and bus #6, see Figure 5.15. This is a severe fault that leads to inter-area oscillations.

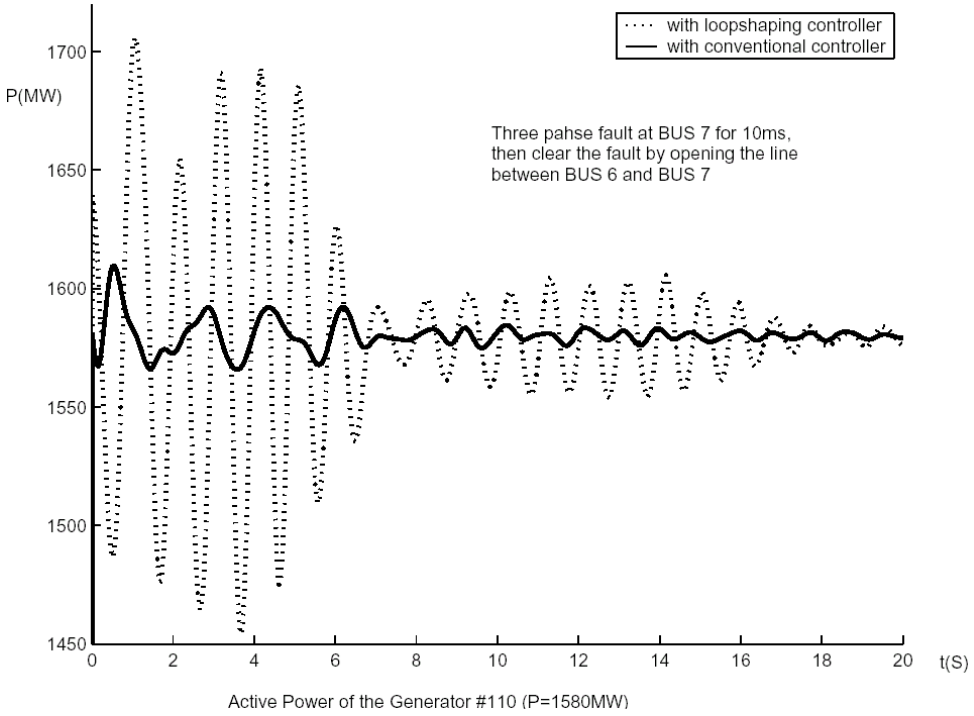

Fig. 5.15 Comparison of the performance between the H_∞ loop shaping controller and the conventional PSS.

These results clearly demonstrate the efficacy of the loop-shaping approach in designing controls with a high degree of robustness and desired performance characteristics. The design procedure is computationally efficient and provides a systematic approach to design controllers in a non-iterative fashion. We have also effectively demonstrated the ability of the technique to perform a sequential design of PSS at different locations for a moderately large system.

References

[1] J. C. Doyle and G. Stein, "Multivariable Feedback Design: Concepts for a Classical/Modern Synthesis," *IEEE Transactions on Automatic Control*, Vol. 26, no. 1, pp. 1-16, 1981.

[2] Duncan McFarlane and Keith Glover, "A Loop Shaping Design Procedure Using H_∞ Synthesis," *IEEE Transactions on Automatic Control*, Vol. 37, no. 6, pp. 759-769, June 1992.

[3] Miodrag Djukanovic, Mustafa Khammash, and Vijay Vittal, "Application of the Structured Singular Value Theory for Robust Stability and Control Analysis in Multi-machine Power Systems, Part I: Framework Development and Part II: Numerical Simulation and Results," *IEEE Transactions on Power Systems*, Vol. 13, pp. 1311–1316, November 1998.

[4] G. J. Balas, J. C. Doyle, K. Glover, A. Packard and R. Smith, *μ Analysis and Synthesis Toolbox User's Guide*, Natick, Mass., Mathwork, 1993.

[5] M. K. H. Fan, A. L. Tits and J. C. Doyle, "Robustness in the Presence of Mixed Parametric Uncertainty and Unmodeled Dynamics," *IEEE Transactions on Automatic Control*, Vol. 36, pp. 25-38, 1991.

[6] J. C. Doyle and A. Packard, "Uncertain Multivariable System from a State Space Perspective," 1987 ACC, pp. 2147-2152.

[7] P. M. Young, "Robustness with Parameter and Dynamic Uncertainty," Ph.D. dissertation, Cal. Ins. of Tech., 1993.

[8] J. C. Doyle, "Analysis of Feedback Systems with Structured Uncertainty," *IEE Proceedings*, Part D, Vol. 129, pp. 242-250, November 1982.

[9] P. M. Anderson and A. A. Fouad, *Power System Control and Stability*, IEEE Press, 1994.

[10] P. Kundur, G. J. Rogers, and D. Y. Wong, "Extended Transient Midterm Stability Program Package: Version 2.0, User's Manuals," ERPI EL-6648, December 1989.

[11] V. Vittal, M. Khammash and M. Djukanovic, "Robust Analysis and Design of Control in Power Systems," EPRI TR-111922, Dec. 1998.

[12] IEEE Committee Report, "Excitation System Models for Power System Stability Studies," *IEEE Transactions on Power Apparatus and Systems,* Vol. PAS-100, pp. 494-509, February 1981.

[13] P. Kundur, M. Klein, G. J. Rogers and M. Zwyno, "Applications of Power System Stabilizers for Enhancement of Overall System Stability," *IEEE Transactions on Power Systems*, Vol. 4, no. 2, pp. 614-622, May 1989.

[14] V. Vittal, "Transient Stability Test Systems for Direct Stability Methods," *IEEE Transactions on Power Apparatus and Systems,* Vol. 7, no. 1, pp. 37-42, February 1992.

[15] S. Skogestad and I. Postlethwaite, *Multivariable Feedback Control Analysis and Design*. Chichester: John Wiley & Sons, 1998.

[16] Sideris, "Elimination of Frequency Search from Robustness Tests," *IEEE Transactions on Automatic Control*, Vol. 37, no. 10, pp. 1635-1640, 1992.

[17] Rod Holland and Peter Young. *A Skew μ Lower Bound*. In *Proceedings of the American Control Conference,* pp. xxx-xxx, 2002.

[18] E. E. Osborne. *On Preconditioning of Matrices*. *Journal of the Association for Computing Machinery*, 7:338-345, 1960.

[19] S. Boyd, L. El Ghaoui, E. Feron and V. Balakrishnan. *Linear Matrix Inequalities in System and Control Theory*. SIAM, 1994.

[20] Duncan McFarlane and Keith Glover, "A Loop Shaping Design Procedure Using H_∞ Synthesis," *IEEE Transactions on Automatic Control*, Vol. 37, no. 6, pp. 759-769, June 1992.

[21] P. Ambos, G. Duc and C. M. Falinower, "Loop Shaping H_∞ Design Applied to the Steam Generator Level Control in EDF Nuclear Power Plant," *Proceedings of the 1996 IEEE Int. Conf. on Control App.*, Dearborn, MI, September 15-18, 1996.

[22] R. F. Pannett, P. K. Chawdhry and C. R. Burrows, "Alternative Robust Control Strategies for Disturbance Rejection in Fluid Power Systems," *Proceedings of the ACC*, San Diego, CA, June 1999.

[23] Graham Rogers, *Power System Oscillations*, Kluwer Academic Publishers, 2000.

[24] P. Kundur, G. J. Rogers and D. Y Wong, "Extended Transient Midterm Stability Program Package: Version 2.0, User's Manuals," EPRI EL-6648, December 1989.

[25] P. Kundur, M. Klein, G. J. Rogers, and M. Zwyno, "Applications of Power System Stabilizers for Enhancement of Overall System Stability," *IEEE Transactions on Power Systems*, Vol. 4, no. 2, pp. 614-622, May 1989.

[26] Tryphon T. Georgiou and Malcolm C. Smith, "Optimal Robustness in the Gap Metric," *IEEE Transaction on Automatic Control*, Vol. 35, pp.673-686, 1990.

[27] P. Kundur, *Power System Stability and Control*, New York: McGrawHill, Inc., 1993.

[28] Chuanjiang Zhu, "Robustness Analysis for Power Systems Based on the Structured Singular Value Tools and the Gap Metric," Ph.D. dissertation, Iowa State University, 2001.